REGULATORY DNA SEQUENCE DESIGN WITH REINFORCEMENT LEARNING

Anonymous authors
Paper under double-blind review

ABSTRACT

Cis-regulatory elements (CREs), such as promoters and enhancers, are relatively short DNA sequences that directly regulate the expression of specific genes. The fitness of CREs, i.e., their functionality to enhance gene expression, highly depend on its nucleotide sequence, especially the composition of some special motifs known as transcription factor binding sites (TFBSs). Designing CREs to optimize their fitness is crucial for therapeutic and bioengineering applications. Existing CRE design methods often rely on simple strategies, such as iteratively introducing random mutations and selecting variants with high fitness from a large number of candidates through an oracle, i.e., a pre-trained gene expression prediction model. Due to the vast search space and lack of prior biological knowledge guidance, these methods are prone to getting trapped in local optima and tend to produce CREs with low diversity. In this paper, we propose the first method that leverages reinforcement learning (RL) to fine-tune a pre-trained autoregressive (AR) generative model for designing high-fitness cell-type-specific CREs while maintaining sequence diversity. We employ prior knowledge of CRE regulatory mechanisms to guide the optimization by incorporating the role of TFBSs into the RL process. In this way, our method encourages the removal of repressor motifs and the addition of activator motifs. We evaluate our method on enhancer design tasks for three distinct human cell types and promoter design tasks in two different yeast media conditions, demonstrating its effectiveness and robustness in generating high-fitness CREs.

1 INTRODUCTION

Cis-regulatory elements (CREs), such as promoters and enhancers, are short functional DNA sequences that regulate gene expression in a cell-type-specific manner. Promoters determine when and where a gene is activated, while enhancers boost gene expression levels. Over the past decade, millions of putative CREs have been identified, but these naturally evolved sequences only represent a small fraction of the possible genetic landscape and are not necessarily optimal for specific expression outcomes. It is crucial to design synthetic CREs with desired fitness (measured by their ability to enhance gene expression) as they have broad applications in areas such as gene therapy (Boye et al., 2013), synthetic biology (Shao et al., 2024), precision medicine (Collins & Varmus, 2015), and agricultural biotechnology (Gao, 2018).

Previous attempts to explore alternative CREs have relied heavily on directed evolution, which involves iterative cycles of mutation and selection in wet-lab settings (Wittkopp & Kalay, 2012; Heinz et al., 2015). This approach is sub-optimal due to the vastness of the DNA sequence space and the significant time and cost required for experimental validation. For example, a 200 base pair (bp) DNA sequence can have up to 2.58×10^{120} possible combinations (Gosai et al., 2024), far exceeding the number of atoms in the observable universe. Thus, efficient computational algorithms are needed to narrow down the design space and prioritize candidates for wet-lab testing.

Advances in high-throughput sequencing technologies, such as massively parallel reporter assays (MPRAs) (de Boer et al., 2020; Vaishnav et al., 2022), have enabled the screening of large libraries of random DNA sequences and the measurement of their activity in specific cell types. Recent studies have begun using fitness prediction models as oracles to guide CRE optimization, enabling the exploration of sequences that outperform naturally occurring ones (Vaishnav et al., 2022; de Almeida

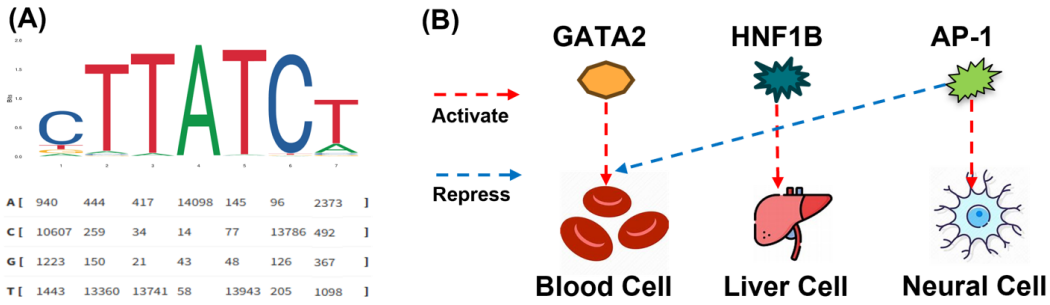

Figure 1: (A) TFBS are commonly represented as frequency matrices, indicating the probability of each nucleotide appearing at specific positions within the binding site. (B) GATA2 and HNF1B specifically activate gene expression in blood cells and liver cells, respectively, while REST specifically represses gene expression in neural cells.

et al., 2024). These methods typically rely on straightforward optimization approaches, such as genetic algorithms or greedy-based directed evolution, which involve two iterative steps: randomly mutating sequences selected in the previous step to form candidates and selecting those with high fitness through an oracle. The entire search space of all possible candidates is vast, but the exploration in each step is performed by heuristic random mutations. Neither empirically learned policies nor any prior biological knowledge are used to guide exploration. As a consequence, these methods are prone to getting trapped in local optima and the produced CREs tend to lack diversity and interpretability.

Inspired by the success of using Reinforcement Learning (RL) for finetuning autoregressive (AR) generative language models (Ouyang et al., 2022; Liu et al., 2024), we propose the first RL finetuning for AR model to design cell-type-specific CREs. We pretrain state-of-the-art (SOTA) AR DNA generative models HyenaDNA (Nguyen et al., 2024b; Lal et al., 2024) on CREs to capture their authentic distribution, ensuring the generation of realistic and diverse CRE sequences. During RL finetuning, we treat the current AR model as the policy network, and utilize the fitness predicted by an oracle as the reward signal. This allows us to update the model parameters to generate CRE sequences that not only maintain diversity but also exhibit high fitness.

Additionally, we incorporate domain knowledge of CREs into our RL process. The regulatory syntax of CREs is largely dictated by the transcription factors (TFs) that bind to them (Gosai et al., 2024; de Almeida et al., 2024; Lal et al., 2024; Zhang et al., 2023). TFs are proteins that directly influence gene expression by binding to specific sequence motifs within CREs, known as TF binding sites (TFBSs), and modulating transcriptional activity. For instance, Fig. 1(A) shows the motif pattern recognized by the GATA2 TF. Furthermore, the effects of TFs can vary widely depending on the cell type. As shown in Fig. 1 (B), GATA2 and HNF1B are TFs that specifically activate gene expression in blood cells and liver cells (Lal et al., 2024), respectively, while REST acts as a repressor of gene expression in neural cells (Zullo et al., 2019), illustrating the cell-type-specific nature of TF activity. More details about the datasets and model can be found in Appendix B and Appendix C. The method for TFBS scanning can be found in Appendix E.

Model	yeast		human		
	complex	defined	hepg2	k562	sknsh
Enformer (Sequence Feature)	0.87	0.91	0.83	0.85	0.85
LightGBM (TFBS Frequency Feature)	0.63	0.65	0.65	0.65	0.66

Table 1: **Pearson correlation coefficient of the Oracle on the test set**. Enformer is a SOTA DNA backbone model that uses DNA sequences as input, while LightGBM is a simple tree model that uses TFBS occurrence frequencies as input.

The effect of a TF can be broken down into its intrinsic role as an activator or repressor (referred to as its "vocabulary") and its interactions with other TFs (such as composition and arrangement). We found that simply using the frequency of TFBS occurrences within a sequence as features can achieve reasonably good fitness prediction performance when trained with a decision tree model LightGBM (Ke et al., 2017). As shown in Tab. 1, the current SOTA DNA model, Enformer, achieves a Pearson correlation of 0.83 on the test set for predicting fitness in the HepG2 cell line using sequence data as input. In contrast, using only simple TFBS frequency features—without any explicit sequence information—achieved a Pearson correlation of 0.65. This demonstrates that even without

leveraging sequence details, TF frequency alone can capture a significant portion of the predictive power. Furthermore, we use the trained LightGBM (Ke et al., 2017) model to infer whether each TFBS feature promotes or represses fitness, which allows us to explicitly incorporate TFBS domain knowledge into our RL process. We name our proposed method **TACO**: **T**FBS-**A**ware ***C**is-Regulatory* Element **O**ptimization, which integrates RL finetuning of AR models with domain knowledge of TFBSs to enhance CRE optimization.

Our main contributions are as follows: (1) We are the first to introduce the RL fine-tuning paradigm to pretrained AR DNA models for CRE design, enabling the generated sequences to maintain high diversity while exploring those with higher functional performance. (2) We incorporate key TFBS information by inferring their regulatory roles and directly integrating their impact into the generation process, facilitating joint data-driven and knowledge-driven exploration guidance. (3) We evaluate our approach on real-world datasets, including yeast promoter designs under two media and human enhancer designs across three cell lines. Not only do we demonstrate the effectiveness of TACO, but we also validate the impact of our core contributions through detailed ablation experiments."

2 Related Work

Conditional DNA Generative Models. DDSM (Avdeyev et al., 2023) was the first to apply diffusion models to DNA design. By leveraging classifier-free guidance Ho & Salimans (2022), the model conditioned DNA sequences on promoter expression levels. Following this, several works have employed diffusion models for CRE design Li et al. (2024b); DaSilva et al. (2024); Sarkar et al. (2024). In addition to diffusion models, regLM (Lal et al., 2024) utilized prefix-tuning on the AR DNA language model HyenaDNA (Nguyen et al., 2024b), incorporating tokens that encode expression strength to fine-tune the model specifically for CRE design. However, these generative methods are designed to fit existing data distributions, limiting their ability to design sequences that have yet to be explored by humans.

DNA Sequence Optimization. DyNA PPO (Angermueller et al., 2019) was an early exploration of applying modern RL to biological sequence design. By improving the sampling efficiency of PPO (Schulman et al., 2017) and leveraging an AR policy, it provided a general framework for biological sequence design. DyNA PPO and its subsequent works (Jain et al., 2022; Zeng et al., 2024) primarily focused on advancing general-purpose sequence design algorithms, with an emphasis on optimizing short TFBS motifs (6-8 bp) in the context of DNA sequence design. .With the availability of larger CRE fitness datasets, Vaishnav et al. (2022) applied genetic algorithms to design CREs. Recent works, such as Gosai et al. (2024), explored greedy approaches like AdaLead (Sinai et al., 2020), simulated annealing (Van Laarhoven et al., 1987), and gradient-based SeqProp (Linder & Seelig, 2021). Similarly, Taskiran et al. (2024) combined greedy strategies with directed evolution. However, these methods often start from random sequences, generating biologically irrelevant sequences, or begin with observed high-fitness sequences, leading to local optima and limited diversity. Our method builds on prior work by incorporating domain knowledge to better explore valid and high-fitness regions in the DNA space. This includes starting from a CRE-pretrained generative model and using biologically inspired TFBS soft rewards for CRE-specific design. Further, Reddy et al. (2024) proposed directly optimizing CREs using gradient ascent (GAs) on a differentiable surrogate trained on offline CRE datasets. They trained a reliable surrogate with regularization to ensure the outputs of GAs are trustworthy and evaluated the sequences on an independently trained oracle. Beyond the methodological contributions, Reddy et al. (2024) validated their approach through *in vitro* experiments, demonstrating the potential of machine learning techniques to discover suitable cell-type-specific CREs in real-world scenarios."

3 Method

3.1 Problem Formulation

We define a DNA sequence $x = (x_1, \cdots, x_L)$ as a string of nucleotides with length L, where $x_i \in \mathcal{V}$ is the nucleotide at the i-th position, and $\mathcal{V}$ is the vocabulary of 4 nucleotides (A, T, C, G). In our CRE optimization task, we assume the availability of a large-scale dataset of CRE sequences

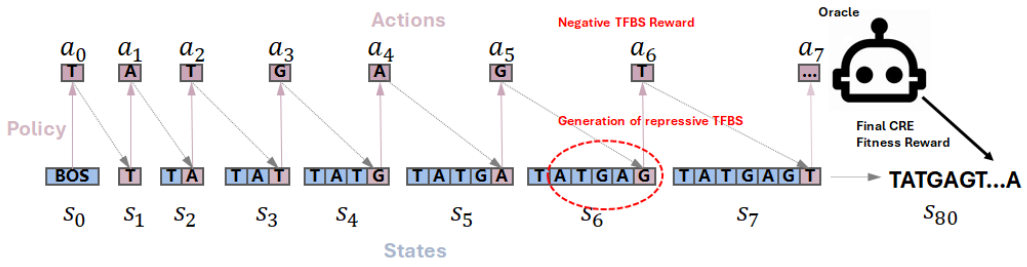

Figure 2: **The autoregressive generation of a DNA sequence.** An AR model for sequence generation can be viewed as an RL policy, where the actions a_t represent the next nucleotides to be appended to the sequence, and the state is the concatenation of all actions taken up to time $t-1$. If an action generates a TFBS that is known to be repressive, a negative reward is given. Conversely, generating a TFBS with activating properties results in a positive reward. The final sequence is evaluated using an oracle to obtain a fitness reward. BOS stands for the beginning of the sequence, and ATCG represents the nucleotide bases.

with fitness measurements $\mathcal{D} = \{(x^1, f(x^1)), \cdots, (x^N, f(x^N))\}$ to train an ideal *in-silico* oracle q_θ, where N is the number of sequences in the dataset and $f(x)$ represents the fitness measurement for sequence x. Here, we use the term *fitness* to denote the desired regulatory activity of a CRE sequence. We follow the setting used in protein optimization (Kirjner et al., 2023; Lee et al., 2024) by sampling a set of low-fitness sequences $\mathcal{D}^*$ from $\mathcal{D}$, which includes only sequences with fitness values below a certain percentile of $\mathcal{D}^*$.

3.2 RL-Based Finetuning for Autoregressive DNA Models

Pretraining AR Model. We pretrain an AR model starting from the released HyenaDNA weights (Nguyen et al., 2024b) on the low-fitness dataset $\mathcal{D}^*$. HyenaDNA achieves strong performance on DNA-related tasks by maintaining both linear complexity and high accuracy (More details in Appendix C). However, as HyenaDNA was originally trained on relatively long human genomic sequences, there exists a length gap between these sequences and the relatively shorter CRE sequences in our task. To address this gap, we continue training the HyenaDNA model on $\mathcal{D}^*$, fine-tuning it to better handle the specific sequence lengths in our dataset (See Appendix Tab. 8).

The pretrained AR model, denoted as π_θ, is trained to predict the probability distribution of the next nucleotide given the preceding sequence. This is achieved by minimizing the negative log-likelihood loss:

$$\min_\theta \mathbb{E}_{x\sim\mathcal{D}^*}\left[\sum_{t=1}^{L} -\log \pi_\theta(a_t = A_t \mid A_{t-1}, \cdots, A_0)\right], \tag{1}$$

where a_t is the nucleotide at position t, and $A_0, \cdots, A_{t-1}$ represent the preceding sequence.

where A_t represents the nucleotide at position t, which corresponds to the action a_t taken by the model. This alignment ensures that the notation for nucleotides is consistent with the actions in the RL setting. Pretraining on $\mathcal{D}^*$ helps the policy learn to generate sequences that already resemble the true CRE distribution (Jin et al., 2020; Chen et al., 2021), providing a good initialization for RL finetuning and promoting diversity in the generated sequences. Moreover, using the generative model as the policy ensures that the generated CREs maintain high diversity throughout the optimization process.

RL-Based Finetuning for AR DNA Models. Next, we formulate the RL finetuning process as a Markov Decision Process (MDP), as illustrated in Fig. 2. In this formulation, the states s_t correspond to the partial sequences generated up to time step t, while the actions a_t represent the nucleotides selected by the policy π_θ. The reward $r(s_t, a_t)$ is defined as a combination of two types of rewards: TFBS reward r_{TFBS} and fitness reward r_{fitness}, as shown in equation 2:

$$r(s_t, a_t) = \begin{cases} r_{\text{fitness}}, & \text{if } t = T, \\ r_{\text{TFBS}}(t), & \text{if } a_t \text{ results in a TFBS } t \in \mathcal{T}, \\ 0, & \text{otherwise.} \end{cases} \tag{2}$$

Here, r_{fitness} is applied when t is the final time step of the episode ($t = T$), and represents the fitness value of the generated sequence as evaluated by the oracle. On the other hand, r_{TFBS} is a reward applied whenever a TFBS $t \in \mathcal{T} = \{t_1, t_2, t_3, \ldots, t_n\}$ is identified in the sequence after selecting a_t. Details on how TFBSs are identified can be found in Appendix E. The specific values of $r_{\text{TFBS}}(t)$ are discussed in Subsec. 3.3. Negative rewards are assigned for generating repressive TFBSs, while positive rewards are given for generating activating TFBSs, as shown in Fig. 2. The overall objective is to maximize the expected cumulative reward:

$$\max_{\theta} J(\theta) = \mathbb{E}_{\pi_\theta} \left[\sum_{t=1}^{T} r(s_t, a_t) \right], \tag{3}$$

where $J(\theta)$ represents the expected cumulative reward, T is the length of the episode, and $r(s_t, a_t)$ is the reward at each time step. This setup ensures that the AR model can learn to generate DNA sequences with the desired regulatory properties by leveraging both sequence structure and domain-specific knowledge of TFBS vocabulary.

Supporting RL Designs. To optimize the policy π_θ, we employ the REINFORCE algorithm (Williams, 1992). Similar to previous studies in molecule optimization (Ghugare et al., 2024), we observed that REINFORCE achieves better results than PPO (Schulman et al., 2017) for DNA sequence generation tasks. Additionally, we leverage a hill climbing replay buffer (Blaschke et al., 2020), which stores and samples high-fitness sequences during training to further guide exploration. We also apply entropy regularization (Ghugare et al., 2024) in the form of $-\frac{1}{\log \pi(a|s)}$, which penalizes actions with excessively high probabilities, thereby discouraging overconfident actions and promoting exploration of less likely ones. This combination of techniques allows the model to effectively balance exploration and exploitation, resulting in improved performance on complex DNA optimization tasks. Detailed ablation experiments supporting this can be found in Appendix I.2.

3.3 Inference of TFBS Regulatory Roles

As illustrated in Fig. 3, our approach to inferring TFBS regulatory roles consists of two steps. First, we train a decision tree-based fitness prediction model using TFBS frequency features as input. Second, we leverage model interpretability techniques to determine the regulatory impact of each TFBS feature.

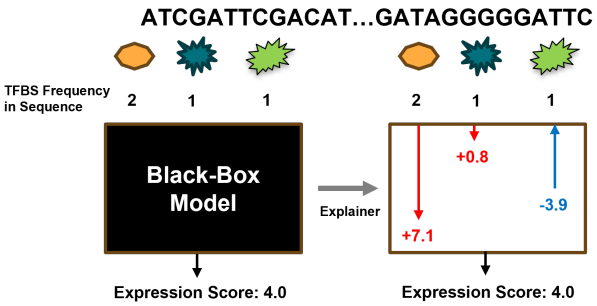

Figure 3: A black-box LightGBM model takes TFBS occurrences as input, and SHAP values infer their contributions to gene expression prediction.

To infer the regulatory impact of each TFBS, we first define the TFBS frequency feature of a sequence x as a vector $\mathbf{h}(x) = [\mathbf{h}_1(x), \mathbf{h}_2(x), \ldots, \mathbf{h}_n(x)]$, where $\mathbf{h}_i(x)$ denotes the frequency of the i-th TFBS in sequence x. This feature vector represents the occurrence pattern of TFBSs within the sequence, making it suitable for tabular data modeling. Details on extracting TFBS features by scanning the sequence can be found in Appendix E. Given the tabular nature of this data, we employ LightGBM (Ke et al., 2017), a tree-based model known for its interpretability and performance on tabular datasets, to fit the fitness values of sequences. LightGBM is chosen because decision tree models, in general, offer better interpretability by breaking down the contribution of each feature in a clear, hierarchical manner. Details of the LightGBM model can be found in Appendix F.

After training, we evaluate the model's performance using the Pearson correlation coefficient between the true and predicted fitness values, as shown in Tab. 1. This evaluation metric helps us quantify how well the LightGBM model captures the relationship between TFBS frequencies and fitness values.

Based on the trained LightGBM model, we use SHAP values (Lundberg, 2017) to interpret the impact of each TFBS on the predicted fitness. SHAP values provide a theoretically grounded approach to attribute the prediction of a model to its input features by calculating the contribution of each feature (in our case, each TFBS) to the prediction. The SHAP value for the i-th TFBS in sequence x, denoted as $\phi_i(x)$, is computed as:

$$\phi_i(x) = \sum_{S \subseteq \{1,\ldots,n\} \setminus \{i\}} \frac{|S|!(n - |S| - 1)!}{n!} \left(f(S \cup \{i\}) - f(S) \right), \tag{4}$$

where S is a subset of features not containing i, $f(S \cup \{i\})$ is the model prediction when feature i is included, and $f(S)$ is the prediction when feature i is excluded. This equation ensures that SHAP values fairly distribute the impact of each feature according to its contribution.

To infer the reward $r_{\text{TFBS}}(t)$ for each TFBS $t \in \mathcal{T} = \{t_1, t_2, t_3, \ldots, t_n\}$, we compute the mean SHAP value of t over the entire dataset. If the mean SHAP value does not significantly differ from zero (p-value > 0.05, determined by hypothesis testing), we set the reward of t to zero:

$$r_{\text{TFBS}}(t) = \begin{cases} \alpha \cdot \mu_\phi(t), & \text{if } p\text{-value} < 0.05, \\ 0, & \text{otherwise}, \end{cases} \tag{5}$$

where α is a tunable hyperparameter, and $\mu_\phi(t)$ is the mean SHAP value of TFBS t across the dataset. This approach ensures that only statistically significant TFBSs contribute to the reward, and α controls the magnitude of the reward.

3.4 Summary of Our Mehod

To summarize, our method integrates two key components. First, we fine-tune an AR generative model, pretrained on CRE sequences, using RL to optimize sequence generation (see Fig. 2). Second, we employ a data-driven approach to infer the role of TFBSs in a cell-type-specific context within the dataset (see Fig. 3). These inferred roles are seamlessly incorporated into the RL process. The complete workflow, detailing the interplay between these components, is presented in Appendix I Alg. 1.

4 Experiment

4.1 Experiment Setup

Datasets and Oracles. We conduct experiments on both yeast promoter and human enhancer datasets. The yeast promoter dataset includes two types of growth media: complex (de Boer et al., 2020) and defined (Vaishnav et al., 2022). The human enhancer dataset consists of three cell lines: HepG2, K562, and SK-N-SH (Gosai et al., 2024). All paired CRE sequences and their corresponding fitness measurements were obtained from massively parallel reporter assays (MPRAs) (Sharon et al., 2012). Our dataset partitioning strategy is based on Lal et al. (2024) Appendix B). The DNA sequence length in the yeast promoter dataset is 80, while it is 200 for the human enhancer dataset.

Each dataset represents a cell-type-specific scenario due to distinct TF effect vocabularies and regulatory landscapes. To simulate optimization from low-fitness CREs, we employ fitness predictors trained on the complete dataset D as oracles (Lal et al., 2024). These oracles guide the optimization process of an AR model that is pretrained on a subset of sequences, D^*, within a specified fitness range. We partition each dataset into three subsets—easy, middle, and hard—based on their fitness values. Detailed partitioning strategies are provided in Appendix B. We set the maximum number of optimization iterations to 100, with up to 256 oracle calls allowed per iteration.

Baselines. We compare our method, TACO, against several established optimization approaches, including Bayesian optimization as implemented in the FLEXS benchmark (Sinai et al., 2020), and evolutionary algorithms such as AdaLead (Sinai et al., 2020) and PEX (Anand & Achim, 2022), as well as covariance matrix adaptation evolution strategy (CMAES) (Auger & Hansen, 2012) using one-hot encoding. Additionally, we adapt the SOTA protein optimization method LatProtRL (Lee et al., 2024) for CRE optimization. Given the lack of a powerful backbone model like ESM (Jain et al., 2022) in the DNA domain (Detailed evidence is provided in Appendix D.2), we remove the ESM-based latent vector encoding from LatProtRL and refer to the resulting model as DNARL. DNARL can be viewed as a sequence mutation-based PPO algorithm (Schulman et al., 2017) enhanced with a replay buffer mechanism. We do not compare with GAs-based approaches (Reddy et al., 2024), as our method and other baselines do not rely on differentiable surrogates. For a detailed discussion on GAs, please refer to Appendix N.

Evaluation Metrics We employ three evaluation metrics: Top, Medium, and Diversity. Top is defined as the mean fitness value of the top 16 sequences (Lee et al., 2024) in the optimized set $\mathcal{G}^* = \{g_1^*, \cdots, g_K^*\}$, highlighting the highest-performing sequences in terms of fitness. Both Medium and Diversity are calculated based on the top $K = 128$ generated sequences, which are selected based on their highest fitness values from a total of 256 sequences generated in each iteration (Lee et al., 2024). Medium refers to the median fitness value among these top 128 sequences, while Diversity is calculated as the median pairwise distance between every pair of these sequences in $\mathcal{G}^*$, providing a measure of variability among the best-performing sequences. These metrics are consistent with those used in LatProtRL (Lee et al., 2024), except for the Novelty metric. We omit Novelty because, unlike proteins, DNA sequences lack well-defined structural constraints, making novelty values disproportionately high and less meaningful. For further details, refer to Appendix G.

Implementation Details. We base the architecture of AR model, i.e., the policy network, on HyenaDNA-1M[1]. We pre-train all initial policies on the subset D^* (Lal et al., 2024). We conduct all experiments on a single NVIDIA A100 GPU. During optimization, we set the learning rate to 5e-4 for the yeast task and 1e-4 for the human task. We set the hyperparameter α, which controls the strength of the TFBS reward in equation 5, to 0.01. We min-max normalize all reported fitness values and the rewards used for updating the policy, while the oracles are trained on the original fitness values.

4.2 Fitness Optimization (Guided by the Oracle)

We report the mean and standard deviation of the evaluation metrics across five runs with different random seeds. In this section, our setup follows an active learning paradigm (Lee et al., 2024; Ghugare et al., 2024), i.e., the model has access to a perfect oracle for feedback at each iteration.

Method	Yeast Promoter (Complex)			Yeast Promoter (Defined)		
	Top	Medium	Diversity	Top	Medium	Diversity
PEX	1	1	9.8 (1.48)	1	1	9.8 (2.59)
AdaLead	1	1	7.6 (0.89)	1	1	6.4 (0.55)
BO	1	1	5.6 (5.57)	1	1	5.6 (1.04)
CMAES	0.79 (0.02)	1	30.0 (2.5)	0.44 (0.03)	1	30.4 (2.3)
DNARL	1	1	7.7 (0.48)	1	1	10.2 (1.4)
TACO	1	1	**52.8 (2.77)**	1	1	**49.6 (3.65)**

Table 2: Performance comparison on yeast promoter datasets (hard setting).

Yeast Promoters. As shown in Tab. 2, optimizing yeast promoters is relatively easy, with most methods generating sequences that significantly exceed the dataset's maximum observed fitness values. For such sequences, the results are reported as 1. Therefore, we only present the results for the hard subset, while the complete results are available in Tab. 11. Among the baselines, only CMAES fails to fully optimize sequences to the maximum fitness value, although it demonstrates strong performance in terms of diversity. Our method not only achieves the maximum fitness but also exhibits the highest diversity compared to all other approaches.

[1] https://huggingface.co/LongSafari/hyenadna-large-1m-seqlen-hf

Method	HepG2-easy			HepG2-medium			HepG2-hard		
	Top	Medium	Diversity	Top	Medium	Diversity	Top	Medium	Diversity
PEX	**0.93** (0.02)	**0.89** (0.01)	20.2 (6.57)	**0.89** (0.04)	**0.86** (0.04)	19.2 (7.12)	**0.85** (0.04)	**0.82** (0.02)	16.0 (2.65)
AdaLead	0.76 (0.00)	0.75 (0.00)	5.2 (0.45)	0.75 (0.03)	0.74 (0.03)	12.4 (4.04)	0.74 (0.02)	0.73 (0.02)	8.0 (1.87)
BO	0.66 (0.06)	0.60 (0.09)	41.6 (8.91)	0.63 (0.05)	0.58 (0.05)	42.0 (7.81)	0.68 (0.04)	0.63 (0.08)	39.8 (5.07)
CMAES	0.61 (0.06)	0.42 (0.04)	77.4 (4.04)	0.67 (0.02)	0.43 (0.03)	75.0 (3.24)	0.69 (0.03)	0.43 (0.02)	77.2 (5.17)
DNARL	0.79 (0.07)	0.71 (0.02)	12.2 (0.08)	0.63 (0.14)	0.84 (0.09)	7.32 (0.01)	0.76 (0.04)	0.72 (0.01)	20.0 (3.42)
TACO	0.78 (0.01)	0.75 (0.01)	**131.8** (2.39)	0.76 (0.01)	0.73 (0.01)	**139.4** (7.13)	0.76 (0.01)	0.74 (0.01)	**131.8** (4.27)
Method	**K562-easy**			**K562-medium**			**K562-hard**		
	Top	**Medium**	**Diversity**	**Top**	**Medium**	**Diversity**	**Top**	**Medium**	**Diversity**
PEX	**0.95** (0.01)	**0.93** (0.01)	21.8 (9.68)	0.94 (0.01)	**0.92** (0.01)	14.6 (1.82)	**0.95** (0.01)	**0.92** (0.02)	15.9 (1.34)
AdaLead	0.85 (0.01)	0.84 (0.01)	7.0 (1.00)	0.85 (0.01)	0.84 (0.01)	9.0 (1.87)	0.85 (0.01)	0.84 (0.01)	8.8 (1.64)
BO	0.70 (0.13)	0.65 (0.12)	41.6 (5.32)	0.76 (0.05)	0.70 (0.05)	39.6 (5.55)	0.74 (0.03)	0.70 (0.04)	37.0 (6.52)
CMAES	0.70 (0.05)	0.42 (0.02)	78.8 (4.09)	0.79 (0.03)	0.50 (0.03)	76.0 (3.24)	0.73 (0.05)	0.47 (0.05)	76.8 (4.55)
DNARL	0.89 (0.04)	0.87 (0.01)	23.3 (3.72)	0.90 (0.02)	0.86 (0.01)	26.3 (1.88)	0.89 (0.01)	0.87 (0.02)	17.5 (3.33)
TACO	0.93 (0.00)	0.91 (0.01)	**124.6** (3.51)	0.92 (0.01)	0.90 (0.02)	**126.0** (1.58)	0.93 (0.01)	0.91 (0.01)	**125.6** (2.88)
Method	**SK-N-SH-easy**			**SK-N-SH-medium**			**SK-N-SH-hard**		
	Top	**Medium**	**Diversity**	**Top**	**Medium**	**Diversity**	**Top**	**Medium**	**Diversity**
PEX	0.90 (0.01)	0.86 (0.03)	22.2 (5.93)	**0.92** (0.02)	**0.88** (0.01)	23.8 (7.85)	0.90 (0.02)	0.86 (0.03)	23.0 (2.74)
AdaLead	0.84 (0.08)	0.82 (0.08)	7.4 (1.52)	0.81 (0.06)	0.80 (0.06)	9.4 (3.05)	0.79 (0.05)	0.78 (0.05)	14.4 (4.45)
BO	0.68 (0.07)	0.62 (0.07)	39.8 (7.89)	0.71 (0.08)	0.64 (0.10)	40.4 (4.83)	0.71 (0.06)	0.63 (0.04)	39.9 (6.60)
CMAES	0.73 (0.04)	0.45 (0.02)	77.0 (3.39)	0.74 (0.01)	0.45 (0.03)	76.0 (3.81)	0.74 (0.02)	0.44 (0.03)	76.0 (3.54)
DNARL	0.83 (0.21)	0.80 (0.06)	35.42 (2.99)	0.83 (0.01)	0.81 (0.01)	28.8 (1.93)	0.82 (0.01)	0.81 (0.01)	18.7 (3.21)
TACO	**0.91** (0.01)	**0.87** (0.02)	**133.8** (4.27)	0.90 (0.01)	0.86 (0.01)	**135.0** (2.12)	**0.92** (0.00)	**0.88** (0.01)	**137.4** (1.14)

Table 3: Performance comparison on human enhancer datasets.

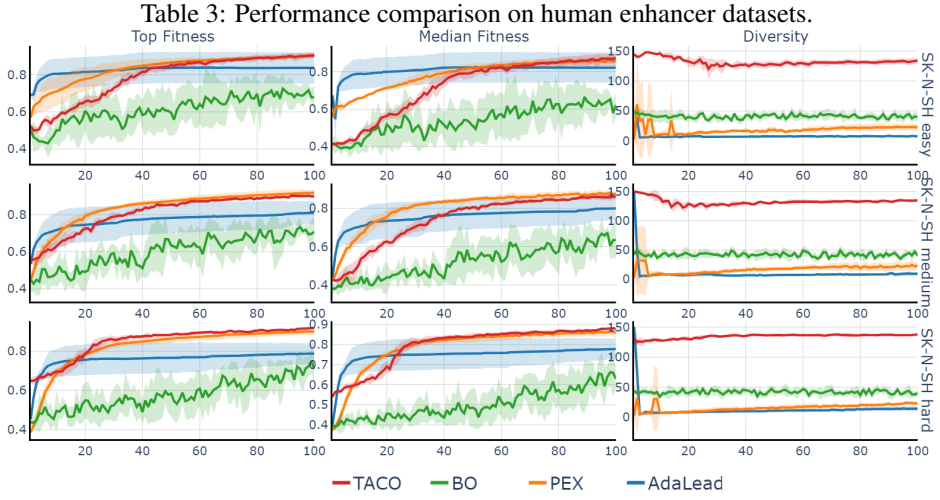

Figure 4: **Evaluation metric by optimization round** for TACO, BO, PEX and Adalead. Shaded regions indicate the standard deviation of 5 runs. The x-axis indicates the number of rounds.

Human Enhancers. Optimizing human enhancers presents a more challenging task. As shown in Appendix Tab. 6, the 90th percentile min-max normalized fitness values for HepG2, K562, and SK-N-SH in the real dataset D are 0.4547, 0.4541, and 0.4453, respectively—less than half of the maximum observed. In Tab. 3, our TACO method demonstrates superior performance compared to the baselines. For the HepG2 cell line, PEX achieves the highest fitness score, but its diversity is typically below 20. In contrast, TACO attains SOTA fitness for K562 and SK-N-SH cell lines while maintaining significantly higher diversity across all datasets (over 1/3 higher than CMAES, which has the highest diversity among baselines).

Evaluation by Optimization Round. As shown in Fig. 4, we present the evaluation results after each round of optimization. We observe that AdaLead, a greedy-based algorithm, quickly finds relatively high-fitness sequences at the initial stages. However, its diversity drops rapidly, causing

the fitness to plateau and get stuck in local optima. In contrast, PEX demonstrates a steady increase in fitness, but it consistently maintains a low diversity throughout. Only TACO not only achieves a stable increase in fitness but also maintains high diversity due to its AR model finetuning paradigm, which effectively balances fitness and diversity throughout the optimization process.

4.3 Offline Model-Based Optimization

We delve into offline model-based optimization (MBO) (Reddy et al., 2024), where the dataset $\mathcal{D}$ is partitioned into a subset D_{offline}. This approach diverges from the methodology outlined in Section 3.1 by relying on the surrogate model trained on D_{offline} to drive the optimization process, while the oracle remains inaccessible during optimization and is reserved solely for final evaluation. In this setting, the dataset is no longer divided based on difficulty; instead, all labeled data available for optimization is drawn from D_{offline}. Apart from this modification, all other settings are identical to those in Section 4.2. . The maximum fitness threshold of the offline dataset corresponds to the 95th percentile of the entire dataset's fitness distribution. Details of the dataset's construction can be found in Appendix J.

Given that the oracle is not visible during the optimization process, we can introduce an additional evaluation metric: the average pairwise cosine similarity of the embeddings of the proposed sequences as generated by the oracle model. This metric, referred to as **Emb Similarity**, quantifies the diversity of the final proposed sequences.

Tab. 4 presents the results of various methods on the K562 dataset. Under the offline MBO setting, the performance of all methods degrades compared to the oracle-guided setting, as the optimization is no longer directly driven by the oracle. The overall trends across methods are consistent with those observed in Sec. 4.2. TACO achieves results in Top and Median fitness that are comparable to PEX while significantly outperforming other optimization methods in terms of diversity. The complete offline MBO results for all datasets are presented in Appendix M. The results of lowering the fitness threshold for the offline dataset are presented in Appendix N in Tab.17, Tab.18, and Tab. 19. We also include two conditional generative models, regLM (Lal et al., 2024) and DDSM (Avdeyev et al., 2023) These methods maintain high diversity in the generated sequences; however, the fitness of the generated sequences is generally inferior to that achieved by most optimization methods. See detailed discussion in Appendix L.

Model	Top ↑	Medium ↑	Diversity ↑	Emb Similarity ↓
PEX	**0.76** (0.02)	**0.73** (0.02)	15.8 (4.97)	0.97 (0.01)
AdaLead	0.66 (0.08)	0.58 (0.06)	63.2 (70.01)	0.88 (0.12)
BO	0.71 (0.07)	0.64 (0.08)	43.6 (6.91)	0.87 (0.04)
CMAES	0.66 (0.02)	0.44 (0.03)	79.2 (3.83)	**0.35** (0.03)
reglm	0.69 (0.02)	0.47 (0.01)	**149.60** (0.49)	<u>0.38</u> (0.02)
DDSM	0.43 (0.00)	0.40 (0.00)	93.40 (0.49)	0.80 (0.00)
TACO	<u>0.75</u> (0.09)	<u>0.72</u> (0.10)	<u>102.6</u> (20.14)	0.97 (0.04)

Table 4: Offline MBO results for human enhancers (K562).

4.4 Ablation Study

The effect of Pretraining and TFBS Reward: Using RL to finetune an pretrained AR model and incorporating TFBS reward are our key contributions. Results are shown in Tab. 5.

First, pretraining on real sequences proves to be highly beneficial. While the "w/o Pretraining" setup occasionally discovers sequences with high fitness, it underperforms on the Medium metric by 0.03, 0.12, and 0.03 compared to the second-best result across datasets. This demonstrates that pretraining allows the policy to begin in a relatively reasonable exploration space, enabling it to identify a large number of suitable sequences more efficiently. This is particularly advantageous in scenarios like CRE optimization, where large-scale experimental validation can be conducted simultaneously.

Dataset	Setting	Top ↑	Medium ↑	Diversity ↑	Emb Similarity ↓
HepG2	TACO ($\alpha = 0.01$)	**0.69** (0.03)	**0.60** (0.05)	**141.2** (1.92)	0.82 (0.05)
	w/o Pretraining	0.68 (0.00)	0.55 (0.02)	139.4 (2.30)	0.69 (0.02)
	w/o TFBS Reward	0.66 (0.05)	0.58 (0.07)	140.8 (1.64)	**0.81** (0.05)
	$\alpha = 0.1$	0.65 (0.06)	0.58 (0.06)	138.6 (3.21)	0.86 (0.04)
K562	TACO ($\alpha = 0.01$)	0.75 (0.09)	0.72 (0.10)	102.6 (20.14)	0.97 (0.04)
	w/o Pretraining	0.66 (0.15)	0.59 (0.16)	**103.6** (25.77)	**0.83** (0.14)
	w/o TFBS Reward	0.76 (0.07)	0.71 (0.08)	106.2 (20.90)	0.94 (0.05)
	$\alpha = 0.1$	**0.78** (0.01)	**0.77** (0.01)	82.8 (4.02)	0.99 (0.00)
SK-N-SH	TACO ($\alpha = 0.01$)	0.68 (0.08)	0.62 (0.08)	121.4 (7.86)	0.90 (0.03)
	w/o Pretraining	0.69 (0.02)	0.57 (0.06)	**131.8** (11.17)	**0.74** (0.11)
	w/o TFBS Reward	0.67 (0.06)	0.60 (0.06)	111.6 (12.86)	0.89 (0.04)
	$\alpha = 0.1$	**0.71** (0.01)	**0.65** (0.02)	121.2 (5.45)	0.90 (0.05)

Table 5: Ablation study on the effect of Pretraining and TFBS Reward.

Additionally, incorporating the TFBS reward significantly enhances the Medium performance of TACO, achieving best results across all datasets. The method outperforms the second-best baseline by margins of 0.02, 0.01, and 0.02, respectively. These prior-informed rewards guide the policy to explore a more rational sequence space efficiently. Moreover, the biologically guided TFBS Reward is surrogate-agnostic, with the potential to achieve a similar effect to the regularization applied to surrogates in (Reddy et al., 2024), by avoiding excessive optimization towards regions where the surrogate model gives unusually high predictions. The differences in the top fitness and diversity achieved by various models are relatively minor, with no consistent conclusion.

As the α increases from the default value of 0.01 to 0.1, our method shows improved performance in both Top and Medium metrics for K562 and SK-N-SH datasets. However, this improvement comes at the cost of a rapid drop in diversity. Interestingly, all metrics for the HepG2 dataset worsen as α grows. We hypothesize that this discrepancy arises from the TFBS Reward, precomputed using the LightGBM model, varying across datasets. Therefore, we recommend carefully tuning α in real-world scenarios to balance the trade-offs effectively.

5 Discussion

The effectiveness of TACO can be attributed to two main factors: starting from a pretrained autoregressive generative model and introducing a biologically informed TFBS Reward. However, there are still several areas for improvement in our approach: (1) The TFBS candidates we use are derived from a fixed database, which bounds the upper limit of the TFBS Reward. Exploring data-driven motif mining (Dudnyk et al., 2024) methods may help to expand this limit. (2) Currently, we infer the role of TFs based solely on TFBS occurrences. In reality, interactions between TFs and their orientation can significantly impact their regulatory roles (Georgakopoulos-Soares et al., 2023). Explicitly incorporating these factors to model more complex TF activities could lead to further improvements. (3) Evaluating the validity of generated DNA sequences requires further attention. Since defining what constitutes a valid DNA sequence is more challenging than for molecules or proteins, we need to more carefully assess validity, potentially by incorporating additional metrics because relying solely on a trained oracle is insufficient.

6 Conclusion

Designing CREs is a highly impactful task, and the increasing availability of fitness data makes it increasingly feasible. Current methods often rely on basic optimization strategies such as genetic algorithms and directed evolution, which, while effective, lack the ability to leverage advanced optimization techniques. To address this limitation, we propose TACO, an RL-based approach that fine-tunes an pretrained AR generative model, achieving both high fitness and diversity in CRE design. By incorporating TFBS domain knowledge, TACO offers a promising direction for further advancements in machine-learning-guided CRE optimization.

REFERENCES

Weizhi An, Yuzhi Guo, Yatao Bian, Hehuan Ma, Jinyu Yang, Chunyuan Li, and Junzhou Huang. Modna: motif-oriented pre-training for dna language model. In *Proceedings of the 13th ACM international conference on bioinformatics, computational biology and health informatics*, pp. 1–5, 2022.

Namrata Anand and Tudor Achim. Protein structure and sequence generation with equivariant denoising diffusion probabilistic models. *arXiv preprint arXiv:2205.15019*, 2022.

Christof Angermueller, David Dohan, David Belanger, Ramya Deshpande, Kevin Murphy, and Lucy Colwell. Model-based reinforcement learning for biological sequence design. In *International conference on learning representations*, 2019.

Anne Auger and Nikolaus Hansen. Tutorial cma-es: evolution strategies and covariance matrix adaptation. In *Proceedings of the 14th annual conference companion on Genetic and evolutionary computation*, pp. 827–848, 2012.

Pavel Avdeyev, Chenlai Shi, Yuhao Tan, Kseniia Dudnyk, and Jian Zhou. Dirichlet diffusion score model for biological sequence generation. In *International Conference on Machine Learning*, pp. 1276–1301. PMLR, 2023.

Žiga Avsec, Vikram Agarwal, Daniel Visentin, Joseph R Ledsam, Agnieszka Grabska-Barwinska, Kyle R Taylor, Yannis Assael, John Jumper, Pushmeet Kohli, and David R Kelley. Effective gene expression prediction from sequence by integrating long-range interactions. *Nature methods*, 18 (10):1196–1203, 2021.

Timothy L Bailey, James Johnson, Charles E Grant, and William S Noble. The meme suite. *Nucleic acids research*, 43(W1):W39–W49, 2015.

Gonzalo Benegas, Carlos Albors, Alan J Aw, Chengzhong Ye, and Yun S Song. Gpn-msa: an alignment-based dna language model for genome-wide variant effect prediction. *bioRxiv*, 2023.

Thomas Blaschke, Josep Arús-Pous, Hongming Chen, Christian Margreitter, Christian Tyrchan, Ola Engkvist, Kostas Papadopoulos, and Atanas Patronov. Reinvent 2.0: an ai tool for de novo drug design. *Journal of chemical information and modeling*, 60(12):5918–5922, 2020.

Shannon E Boye, Sanford L Boye, Alfred S Lewin, and William W Hauswirth. A comprehensive review of retinal gene therapy. *Molecular therapy*, 21(3):509–519, 2013.

Binghong Chen, Tianzhe Wang, Chengtao Li, Hanjun Dai, and Le Song. Molecule optimization by explainable evolution. In *International conference on learning representation (ICLR)*, 2021.

Francis S Collins and Harold Varmus. A new initiative on precision medicine. *New England journal of medicine*, 372(9):793–795, 2015.

Lucas Ferreira DaSilva, Simon Senan, Zain Munir Patel, Aniketh Janardhan Reddy, Sameer Gabbita, Zach Nussbaum, César Miguel Valdez Córdova, Aaron Wenteler, Noah Weber, Tin M Tunjic, et al. Dna-diffusion: Leveraging generative models for controlling chromatin accessibility and gene expression via synthetic regulatory elements. *bioRxiv*, 2024.

Bernardo P de Almeida, Christoph Schaub, Michaela Pagani, Stefano Secchia, Eileen EM Furlong, and Alexander Stark. Targeted design of synthetic enhancers for selected tissues in the drosophila embryo. *Nature*, 626(7997):207–211, 2024.

Carl G de Boer, Eeshit Dhaval Vaishnav, Ronen Sadeh, Esteban Luis Abeyta, Nir Friedman, and Aviv Regev. Deciphering eukaryotic gene-regulatory logic with 100 million random promoters. *Nature biotechnology*, 38(1):56–65, 2020.

Kseniia Dudnyk, Donghong Cai, Chenlai Shi, Jian Xu, and Jian Zhou. Sequence basis of transcription initiation in the human genome. *Science*, 384(6694):eadj0116, 2024.

Oriol Fornes, Jaime A Castro-Mondragon, Aziz Khan, Robin Van der Lee, Xi Zhang, Phillip A Richmond, Bhavi P Modi, Solenne Correard, Marius Gheorghe, Damir Baranašić, et al. Jaspar 2020: update of the open-access database of transcription factor binding profiles. *Nucleic acids research*, 48(D1):D87–D92, 2020.

Caixia Gao. The future of crispr technologies in agriculture. *Nature Reviews Molecular Cell Biology*, 19(5):275–276, 2018.

Zijie Geng, Shufang Xie, Yingce Xia, Lijun Wu, Tao Qin, Jie Wang, Yongdong Zhang, Feng Wu, and Tie-Yan Liu. De novo molecular generation via connection-aware motif mining. In *The Eleventh International Conference on Learning Representations*.

Ilias Georgakopoulos-Soares, Chengyu Deng, Vikram Agarwal, Candace SY Chan, Jingjing Zhao, Fumitaka Inoue, and Nadav Ahituv. Transcription factor binding site orientation and order are major drivers of gene regulatory activity. *Nature communications*, 14(1):2333, 2023.

Raj Ghugare, Santiago Miret, Adriana Hugessen, Mariano Phielipp, and Glen Berseth. Searching for high-value molecules using reinforcement learning and transformers. In *The Twelfth International Conference on Learning Representations*, 2024.

Sager J Gosai, Rodrigo I Castro, Natalia Fuentes, John C Butts, Kousuke Mouri, Michael Alasoadura, Susan Kales, Thanh Thanh L Nguyen, Ramil R Noche, Arya S Rao, et al. Machine-guided design of cell-type-targeting cis-regulatory elements. *Nature*, pp. 1–10, 2024.

Sven Heinz, Casey E Romanoski, Christopher Benner, and Christopher K Glass. The selection and function of cell type-specific enhancers. *Nature reviews Molecular cell biology*, 16(3):144–154, 2015.

Jonathan Ho and Tim Salimans. Classifier-free diffusion guidance. *arXiv preprint arXiv:2207.12598*, 2022.

Connie Huang, Richard W Shuai, Parth Baokar, Ryan Chung, Ruchir Rastogi, Pooja Kathail, and Nilah M Ioannidis. Personal transcriptome variation is poorly explained by current genomic deep learning models. *Nature Genetics*, 55(12):2056–2059, 2023.

Moksh Jain, Emmanuel Bengio, Alex Hernandez-Garcia, Jarrid Rector-Brooks, Bonaventure FP Dossou, Chanakya Ajit Ekbote, Jie Fu, Tianyu Zhang, Michael Kilgour, Dinghuai Zhang, et al. Biological sequence design with gflownets. In *International Conference on Machine Learning*, pp. 9786–9801. PMLR, 2022.

Wengong Jin, Regina Barzilay, and Tommi Jaakkola. Multi-objective molecule generation using interpretable substructures. In *International conference on machine learning*, pp. 4849–4859. PMLR, 2020.

Alexander Karollus, Thomas Mauermeier, and Julien Gagneur. Current sequence-based models capture gene expression determinants in promoters but mostly ignore distal enhancers. *Genome biology*, 24(1):56, 2023.

Guolin Ke, Qi Meng, Thomas Finley, Taifeng Wang, Wei Chen, Weidong Ma, Qiwei Ye, and Tie-Yan Liu. Lightgbm: A highly efficient gradient boosting decision tree. *Advances in neural information processing systems*, 30, 2017.

Andrew Kirjner, Jason Yim, Raman Samusevich, Shahar Bracha, Tommi S Jaakkola, Regina Barzilay, and Ila R Fiete. Improving protein optimization with smoothed fitness landscapes. In *The Twelfth International Conference on Learning Representations*, 2023.

Avantika Lal, David Garfield, Tommaso Biancalani, and Gokcen Eraslan. reglm: Designing realistic regulatory dna with autoregressive language models. In *International Conference on Research in Computational Molecular Biology*, pp. 332–335. Springer, 2024.

Minji Lee, Luiz Felipe Vecchietti, Hyunkyu Jung, Hyun Joo Ro, Meeyoung Cha, and Ho Min Kim. Robust optimization in protein fitness landscapes using reinforcement learning in latent space. In *Forty-first International Conference on Machine Learning*, 2024.

Siyuan Li, Zedong Wang, Zicheng Liu, Di Wu, Cheng Tan, Jiangbin Zheng, Yufei Huang, and Stan Z. Li. VQDNA: Unleashing the power of vector quantization for multi-species genomic sequence modeling. In *Forty-first International Conference on Machine Learning*, 2024a.

Zehui Li, Yuhao Ni, William AV Beardall, Guoxuan Xia, Akashaditya Das, Guy-Bart Stan, and Yiren Zhao. Discdiff: Latent diffusion model for dna sequence generation. *arXiv preprint arXiv:2402.06079*, 2024b.

Johannes Linder and Georg Seelig. Fast activation maximization for molecular sequence design. *BMC bioinformatics*, 22:1–20, 2021.

Tianqi Liu, Yao Zhao, Rishabh Joshi, Misha Khalman, Mohammad Saleh, Peter J Liu, and Jialu Liu. Statistical rejection sampling improves preference optimization. In *The Twelfth International Conference on Learning Representations*, 2024.

Scott Lundberg. A unified approach to interpreting model predictions. *arXiv preprint arXiv:1705.07874*, 2017.

Joshua Meier, Roshan Rao, Robert Verkuil, Jason Liu, Tom Sercu, and Alex Rives. Language models enable zero-shot prediction of the effects of mutations on protein function. *Advances in neural information processing systems*, 34:29287–29303, 2021.

Eric Nguyen, Michael Poli, Matthew G Durrant, Brian Kang, Dhruva Katrekar, David B Li, Liam J Bartie, Armin W Thomas, Samuel H King, Garyk Brixi, et al. Sequence modeling and design from molecular to genome scale with evo. *Science*, 386(6723):eado9336, 2024a.

Eric Nguyen, Michael Poli, Marjan Faizi, Armin Thomas, Michael Wornow, Callum Birch-Sykes, Stefano Massaroli, Aman Patel, Clayton Rabideau, Yoshua Bengio, et al. Hyenadna: Long-range genomic sequence modeling at single nucleotide resolution. *Advances in neural information processing systems*, 36, 2024b.

Long Ouyang, Jeffrey Wu, Xu Jiang, Diogo Almeida, Carroll Wainwright, Pamela Mishkin, Chong Zhang, Sandhini Agarwal, Katarina Slama, Alex Ray, et al. Training language models to follow instructions with human feedback. *Advances in neural information processing systems*, 35: 27730–27744, 2022.

Aniketh Janardhan Reddy, Xinyang Geng, Michael H Herschl, Sathvik Kolli, Aviral Kumar, Patrick D Hsu, Sergey Levine, and Nilah M Ioannidis. Designing cell-type-specific promoter sequences using conservative model-based optimization. *bioRxiv*, pp. 2024–06, 2024.

Anirban Sarkar, Ziqi Tang, Chris Zhao, and Peter Koo. Designing dna with tunable regulatory activity using discrete diffusion. *bioRxiv*, pp. 2024–05, 2024.

Yair Schiff, Chia Hsiang Kao, Aaron Gokaslan, Tri Dao, Albert Gu, and Volodymyr Kuleshov. Caduceus: Bi-directional equivariant long-range dna sequence modeling. In *Forty-first International Conference on Machine Learning*.

John Schulman, Filip Wolski, Prafulla Dhariwal, Alec Radford, and Oleg Klimov. Proximal policy optimization algorithms. *arXiv preprint arXiv:1707.06347*, 2017.

Jiawei Shao, Xinyuan Qiu, Lihang Zhang, Shichao Li, Shuai Xue, Yaqing Si, Yilin Li, Jian Jiang, Yuhang Wu, Qiqi Xiong, et al. Multi-layered computational gene networks by engineered tristate logics. *Cell*, 2024.

Eilon Sharon, Yael Kalma, Ayala Sharp, Tali Raveh-Sadka, Michal Levo, Danny Zeevi, Leeat Keren, Zohar Yakhini, Adina Weinberger, and Eran Segal. Inferring gene regulatory logic from high-throughput measurements of thousands of systematically designed promoters. *Nature biotechnology*, 30(6):521–530, 2012.

Sam Sinai, Richard Wang, Alexander Whatley, Stewart Slocum, Elina Locane, and Eric D Kelsic. Adalead: A simple and robust adaptive greedy search algorithm for sequence design. *arXiv preprint arXiv:2010.02141*, 2020.

Ziqi Tang and Peter K Koo. Evaluating the representational power of pre-trained dna language models for regulatory genomics. *bioRxiv*, pp. 2024–02, 2024.

Ibrahim I Taskiran, Katina I Spanier, Hannah Dickmänken, Niklas Kempynck, Alexandra Pančíková, Eren Can Ekşi, Gert Hulselmans, Joy N Ismail, Koen Theunis, Roel Vandepoel, et al. Cell-type-directed design of synthetic enhancers. *Nature*, 626(7997):212–220, 2024.

Masatoshi Uehara, Yulai Zhao, Ehsan Hajiramezanali, Gabriele Scalia, Gökcen Eraslan, Avantika Lal, Sergey Levine, and Tommaso Biancalani. Bridging model-based optimization and generative modeling via conservative fine-tuning of diffusion models. *arXiv preprint arXiv:2405.19673*, 2024.

Eeshit Dhaval Vaishnav, Carl G de Boer, Jennifer Molinet, Moran Yassour, Lin Fan, Xian Adiconis, Dawn A Thompson, Joshua Z Levin, Francisco A Cubillos, and Aviv Regev. The evolution, evolvability and engineering of gene regulatory dna. *Nature*, 603(7901):455–463, 2022.

Peter JM Van Laarhoven, Emile HL Aarts, Peter JM van Laarhoven, and Emile HL Aarts. *Simulated annealing*. Springer, 1987.

Ronald J Williams. Simple statistical gradient-following algorithms for connectionist reinforcement learning. *Machine learning*, 8:229–256, 1992.

Cort J Willmott and Kenji Matsuura. Advantages of the mean absolute error (mae) over the root mean square error (rmse) in assessing average model performance. *Climate research*, 30(1):79–82, 2005.

Patricia J Wittkopp and Gizem Kalay. Cis-regulatory elements: molecular mechanisms and evolutionary processes underlying divergence. *Nature Reviews Genetics*, 13(1):59–69, 2012.

Zhenxing Wu, Jike Wang, Hongyan Du, Dejun Jiang, Yu Kang, Dan Li, Peichen Pan, Yafeng Deng, Dongsheng Cao, Chang-Yu Hsieh, et al. Chemistry-intuitive explanation of graph neural networks for molecular property prediction with substructure masking. *Nature Communications*, 14(1): 2585, 2023.

Tianhao Yu, Haiyang Cui, Jianan Canal Li, Yunan Luo, Guangde Jiang, and Huimin Zhao. Enzyme function prediction using contrastive learning. *Science*, 379(6639):1358–1363, 2023.

Xi Zeng, Xiaotian Hao, Hongyao Tang, Zhentao Tang, Shaoqing Jiao, Dazhi Lu, and Jiajie Peng. Designing biological sequences without prior knowledge using evolutionary reinforcement learning. In *Proceedings of the AAAI Conference on Artificial Intelligence*, volume 38, pp. 383–391, 2024.

Pengcheng Zhang, Haochen Wang, Hanwen Xu, Lei Wei, Liyang Liu, Zhirui Hu, and Xiaowo Wang. Deep flanking sequence engineering for efficient promoter design using deepseed. *Nature communications*, 14(1):6309, 2023.

Zaixi Zhang, Qi Liu, Hao Wang, Chengqiang Lu, and Chee-Kong Lee. Motif-based graph self-supervised learning for molecular property prediction. *Advances in Neural Information Processing Systems*, 34:15870–15882, 2021.

Zhihan Zhou, Yanrong Ji, Weijian Li, Pratik Dutta, Ramana V Davuluri, and Han Liu. DNABERT-2: Efficient foundation model and benchmark for multi-species genomes. In *The Twelfth International Conference on Learning Representations*, 2024.

Joseph M Zullo, Derek Drake, Liviu Aron, Patrick O'Hern, Sameer C Dhamne, Noah Davidsohn, Chai-An Mao, William H Klein, Alexander Rotenberg, David A Bennett, et al. Regulation of lifespan by neural excitation and rest. *Nature*, 574(7778):359–364, 2019.

APPENDIX

A PRELIMINARY ON CREs

What are CREs? CREs are non-coding DNA sequences that regulate the expression of nearby genes by modulating the binding of TFs and RNA polymerase. The two main types of CREs are promoters, which initiate and maintain mRNA transcription, and enhancers, which are distal elements that interact with promoters to increase gene expression. CREs play a crucial role in establishing specific gene expression profiles across different cell types, influencing cellular identity and function.

Why are CREs cell-type specific? The cell-type specificity of CREs arises from differential TF binding. TF binding is influenced by several factors, including DNA sequence composition, local chromatin structure, and interactions with other proteins and cofactors. Human cells express around 1,500 to 2,000 different TFs, and their expression patterns vary across cell types. Each cell type thus has a unique set of active CREs that drive the expression of genes necessary for its specific functions. For example, a CRE active in liver cells (hepatocytes) might bind liver-specific TFs such as HNF4A, whereas in neurons, the same CRE might be inactive due to the absence of these TFs.

How are designed CREs utilized? Designed CREs can be used in both *in-vivo* and *in-vitro* settings depending on the application.*In-vivo*, CREs are often delivered using viral vectors, such as adenoviruses or adeno-associated viruses (AAVs), which facilitate the incorporation of synthetic CREs into the target cell's genome. This method is particularly useful for gene therapy, where precise control over gene expression is crucial for therapeutic efficacy and safety. *In-vitro*, CREs are typically introduced into cultured cells using plasmids or CRISPR-based methods, allowing researchers to test the functionality and regulatory impact of the synthetic CREs under controlled conditions. This approach is invaluable for high-throughput screening of CRE designs and optimization of regulatory elements before moving to *in-vivo* applications.

Applications and Future Prospects. Designing synthetic CREs with precise, cell-type-specific regulatory functions has significant potential in both basic research and therapeutic applications. In gene therapy, cell-type-specific CREs can be used to target therapeutic gene expression to specific tissues, minimizing off-target effects and toxicity. In industrial biotechnology, engineered CREs can optimize protein production in desired cell lines. Recent advances in deep learning and generative models have shown promise in predicting and generating CREs with desired regulatory profiles, opening new avenues for programmable gene regulation.

B DETAILS OF DATASETS

Existing CRE fitness datasets are generated through Massively Parallel Reporter Assays (MPRAs), which allow for high-throughput measurements of regulatory sequences in in vitro settings. The yeast promoter dataset includes results from two different media conditions: *complex* and *defined*. The human enhancer dataset, on the other hand, consists of data from three distinct human cell lines: HepG2 (a liver cell line), K562 (an erythrocyte cell line), and SK-N-SH (a neuroblastoma cell line). As shown in Tab. 6, the 90th percentile min-max normalized fitness values for HepG2, K562, and SK-N-SH in the real dataset D are 0.4547, 0.4541, and 0.4453, respectively.

We adopt the dataset splits proposed by RegLM (Lal et al., 2024) and use their defined training set as our full dataset, denoted as $\mathcal{D}$. To simulate a progression from low-fitness to high-fitness sequences, we further partition $\mathcal{D}$ into a subset $\mathcal{D}^*$ for finetuning and evaluation. Each dataset represents a cell-type-specific scenario due to distinct TF effect vocabularies and regulatory landscapes.

Our partitioning scheme follows the same approach as RegLM. Specifically, we define three difficulty levels—*hard*, *medium*, and *easy*—based on fitness percentiles of 20-40, 40-60, and 60-80, respectively, in both media conditions for the yeast dataset. Since yeast is a single-cell organism, we ensure that the fitness levels are consistent across both media. For the human enhancer datasets, we define the *hard* fitness range as values below 0.2, the *medium* range as values between 0.2 and 0.75, and the *easy* range as values between 0.75 and 2.5. These ranges are selected to maintain fitness values below 0.2 in other cell lines, thereby simulating a cell-type-specific regulatory scenario.

Cell Line	75th Percentile	90th Percentile
HepG2	0.3994	0.4547
K562	0.3975	0.4541
SK-N-SH	0.3986	0.4453

Table 6: Enhancer fitness.

C ENFORMER SERVES AS ORACLE

Enformer (Avsec et al., 2021) is a hybrid architecture that combines CNNs and Transformers, achieving SOTA performance across a range of DNA regulatory prediction tasks. In our study, all CRE fitness prediction oracles are based on the Enformer architecture (Lal et al., 2024; Uehara et al., 2024). The primary distinction lies in the output: while the original Enformer model predicts 5,313 human chromatin profiles, we modify it to predict a single scalar value representing CRE fitness.

The oracle model for the human enhancer datasets retains the same number of parameters as the original Enformer. In contrast, for the yeast promoter datasets, we reduce the model size due to the simpler nature of yeast promoter sequences. Specific architectural configurations are listed in Tab. 7. In this study, we directly utilize the oracle weights provided by regLM (Lal et al., 2024) for consistency.

Model	Dimension	Depth	Number of Downsamples
Human Enhancer	1536	11	7
Yeast Promoter	384	1	3

Table 7: Oracle model parameters for human and yeast datasets.

D DISCUSSION ON DNA FOUNDATION MODELS

Over the past year, there has been significant growth in the development of DNA foundation models, with many new models emerging. However, most of these models, such as Caduceus (Schiff et al.), DNABert2 (Zhou et al., 2024), and VQDNA (Li et al., 2024a), are based on BERT-style pretraining and lack the capability to generate DNA sequences. Among them, HyenaDNA (Nguyen et al., 2024b) is the only GPT-style DNA language model. Unlike traditional Transformer-based architectures, HyenaDNA leverages a state space model (SSM), which provides linear computational complexity, making it suitable for handling long DNA sequences with complex dependencies. Subsequent work based on HyenaDNA, such as Evo (Nguyen et al., 2024a), has demonstrated the powerful DNA sequence generation capabilities of this architecture. Additionally, regLM (Lal et al., 2024) has explored conditional DNA generation by employing a prefix-tuning strategy, where a customized token is used as the prefix of the DNA sequence to guide the subsequent generation process. This approach has enabled reglm to effectively model context-dependent DNA sequence generation.

D.1 EFFECT OF THE TRAINING LENGTH

Although HyenaDNA can serve directly as an initial policy, its pretraining was conducted on sequences with a length of 1M. Therefore, as described in Section 3.2, we fine-tune the initial oracle on CRE data. As shown in Table 8, fine-tuning HyenaDNA on short CRE sequences yields slight improvements in performance. We attribute this improvement to the fine-tuning process exposing the model to more short sequences, which aligns with the sequence lengths required for subsequent CRE design tasks.

Model	Top ↑	Medium ↑
Pretrained HyenaDNA	0.749	0.723
Fine-tuned HyenaDNA	**0.751**	**0.729**

Table 8: Performance (hepg2 hard) comparison of pretrained and fine-tuned HyenaDNA on short CRE sequences.

D.2 Limitations of Current DNA Foundation Mdoels

While there have been advancements in DNA foundation models, evidence suggests that they do not yet match the capabilities of models like ESM (Vaishnav et al., 2022). Specifically: (1) ESM embeddings are known for their high versatility and are widely utilized in various downstream tasks, e.g., enzyme function prediction (Yu et al., 2023). In contrast, as noted in Tang & Koo (2024), DNA foundation model embeddings often **perform no better than one-hot encodings**. (2) ESM's language model head can achieve AUROC scores above 0.9 in pathogenic mutation prediction by directly calculating the log-likelihood ratio of reference and alternative alleles (Meier et al., 2021). However, DNA foundation models currently perform significantly worse, with AUROC scores below 0.6 as reported in Benegas et al. (2023). (3) In addition to sequence-based DNA foundation models, some supervised DNA models have also been shown to exhibit limitations in distinguishing mutations across individuals Huang et al. (2023) and recognizing long-range DNA interactions Karollus et al. (2023).

E TFBS Scan and Frequency Feature Preprocessing

The Jaspar database (Fornes et al., 2020) provides detailed annotations of TFBSs. Each TFBS t_i corresponds to a transcription factor that binds to it, regulating gene expression. Instead of representing t_i as a fixed sequence, it is described by a position frequency matrix $\mathbf{M}_i \in \mathbb{R}^{L_i \times 4}$, where L_i is the length of the TFBS, and the four columns correspond to the nucleotides $\{\mathrm{A}, \mathrm{C}, \mathrm{G}, \mathrm{T}\}$. The matrix encodes the likelihood of each nucleotide appearing at each position in the TFBS, making it possible to capture variations in TF binding.

We utilize FIMO (Find Individual Motif Occurrences) (Bailey et al., 2015) to scan each sequence for potential TFBSs. Given a sequence x and a matrix $\mathbf{M}_i$, FIMO evaluates each subsequence x_j in x by calculating a probabilistic score:

$$\text{score}(x_j, \mathbf{M}_i) = \prod_{k=1}^{L_i} P(n_k \mid \mathbf{M}_i[k]), \tag{6}$$

where $P(n_k \mid \mathbf{M}_i[k])$ represents the probability of nucleotide n_k occurring at position k in the matrix $\mathbf{M}_i$. FIMO identifies the subsequences with the highest scores as potential occurrences of the TFBS.

For each sequence x, FIMO outputs a frequency feature vector $\mathbf{h}(x) = [\mathbf{h}_1(x), \mathbf{h}_2(x), \ldots, \mathbf{h}_n(x)]$, where $\mathbf{h}_i(x)$ denotes the frequency of the i-th TFBS in sequence x. This frequency feature vector is then used as input for the downstream prediction model. The use of frequency-based features, as opposed to binary indicators, captures the varying levels of TFBS occurrences in the sequence, allowing for a more nuanced understanding of the regulatory role of each TFBS. Given this tabular representation, we employ LightGBM (Ke et al., 2017), a tree-based model known for its interpretability and effectiveness on tabular datasets, to predict the fitness values of sequences.

E.1 TFBS Distribution Analysis

We scanned the yeast promoters (Complex and Defined datasets) and human enhancers (HepG2, K562, and SK-N-SH datasets) for TFBS occurrences. Figure 5 and Figure 6 show the Venn diagrams of TFBS overlaps for the yeast and human datasets, respectively.

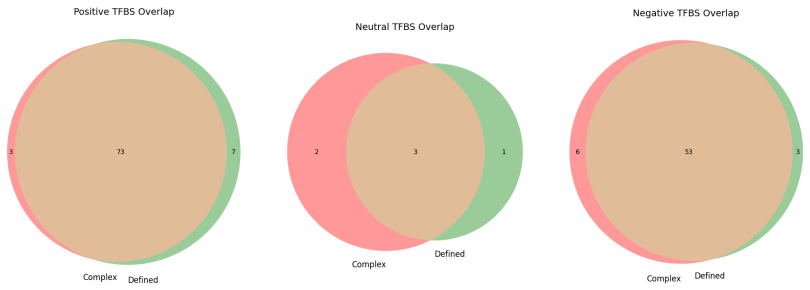

Figure 5: Venn diagram showing TFBS overlap between yeast promoters in two media (Complex and Defined). The TFBS distributions are nearly identical, with minimal differences.

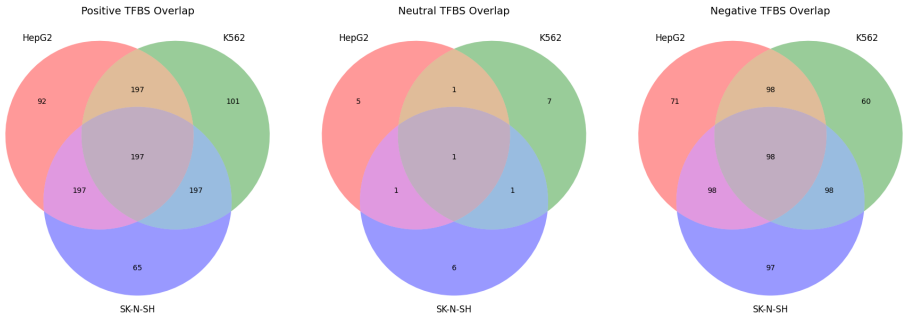

Figure 6: Venn diagrams showing TFBS overlaps for human enhancers across three cell lines (HepG2, K562, and SK-N-SH). The diagrams highlight significant differences in TFBS distribution among the cell lines.

For the yeast promoters, as shown in Figure 5, the TFBS distributions in Complex and Defined datasets are almost identical, with the Venn diagram showing nearly complete overlap. This indicates that the inferred TFBS roles are consistent across the two media, supporting the robustness of our approach in this scenario.

In contrast, the human enhancer datasets (Figure 6) reveal substantial differences in TFBS distributions across the three cell lines. For example, some TFBSs are unique to specific cell lines, while others overlap partially or entirely among the three. This observation underscores the cell-type-specific nature of enhancer regulation and highlights the importance of considering such variability in human enhancer design tasks.

By comparing the yeast and human datasets, we observe that TFBS roles are highly consistent across different conditions in yeast promoters, while human enhancer regulation exhibits greater diversity across cell types. This reinforces the significance of incorporating TFBS-specific insights in designing CREs tailored for human applications.

F Details of LightGBM

We utilized LightGBM (Ke et al., 2017) to train models that directly predict CRE fitness based on TFBS frequency features, enabling us to infer the cell type-specific roles of individual TFBSs. To infer the regulatory impact of each TFBS, we first define the TFBS frequency feature of a sequence x as a vector $\mathbf{h}(x) = [\mathbf{h}_1(x), \mathbf{h}_2(x), \ldots, \mathbf{h}_n(x)]$, where $\mathbf{h}_i(x)$ denotes the frequency of the i-th TFBS in sequence x. The LightGBM model is trained to map the TFBS frequency features to the corresponding fitness values of sequences, using the objective function:

$$\min_{\gamma} \sum_{(\mathbf{h}(x),u(x))\in\mathcal{D}^*} d\left(u(x), \hat{u}(\mathbf{h}(x);\gamma)\right), \tag{7}$$

where $u(x)$ is the true fitness value of sequence x, $\hat{u}(\mathbf{h}(x);\gamma)$ is the fitness value predicted by the LightGBM model parameterized by γ using the TFBS frequency feature vector $\mathbf{h}(x)$. The term $d\left(u(x), \hat{u}(\mathbf{h}(x);\gamma)\right)$ represents a distance metric measuring the discrepancy between the true and predicted fitness values.

For each dataset, we independently trained a LightGBM regression model. The specific parameters used in our model are listed in Table 9.

Parameter	**Value**
Objective	Regression
Metric	MAE
Boosting Type	GBDT
Number of Leaves	63
Learning Rate	0.05
Feature Fraction	0.7
Seed	Random State

Table 9: Hyperparameters used for training the LightGBM regression model.

Metric	**yeast**		**human**		
	complex	**defined**	**hepg2**	**k562**	**sknsh**
MAE	0.63	0.65	0.65	0.65	0.66
RMSE	0.63	0.64	0.56	0.57	0.58

Table 10: Ablation study comparing different metrics on CRE fitness prediction for yeast and human datasets.

We experimented with various metrics corresponding to the metric d in Equation equation 7, specifically testing `rmse` and `mae` as well as different learning rates $\{0.01, 0.05\}$ and number of leaves $\{31, 63\}$. Our preliminary experiments indicate that learning rate and the number of leaves have minimal impact on the results, while the choice of metric significantly affects performance. The results for these two factors are shown in Table 10. This is likely because TFBS occurrences are highly sparse, and MAE tends to perform better with sparse features (Willmott & Matsuura, 2005).

$$d_{\text{MAE}} = \frac{1}{n}\sum_{i=1}^{n}\left|f(x_i) - \hat{f}(h(x_i);\theta)\right| \tag{8}$$

$$d_{\text{RMSE}} = \sqrt{\frac{1}{n}\sum_{i=1}^{n}\left(f(x_i) - \hat{f}(h(x_i);\theta)\right)^2} \tag{9}$$

Our experiments demonstrate that the MAE metric yields better performance across all cell types, as shown in Table 10. Therefore, we selected MAE as the final evaluation metric.

G DNA SEQUENCE PLAUSIBILITY

Unlike molecules and proteins (Uehara et al., 2024), which inherently possess well-defined physical and chemical properties, DNA sequences lack such structural constraints. For example, molecular structures are subject to physical properties like bond angles and energy states, while protein sequences are evaluated based on their 3D folding stability and interactions, making it straightforward to filter out physically implausible designs. Therefore, in molecule and protein design, oracle-predicted fitness is often supplemented with physical property constraints to ensure the plausibility of generated candidates. This helps exclude a significant number of physically infeasible structures, enhancing the relevance of the optimization process.

However, DNA sequences pose a unique challenge in this regard. Unlike molecules or proteins, DNA's plausibility cannot be easily assessed through physical properties, as its functional attributes are primarily determined by its interaction with transcription factors and other regulatory proteins in a context-specific manner. Furthermore, current MPRA (massively parallel reporter assay) datasets are typically generated from random sequences, meaning there is no inherent concept of "plausibility" in the data itself. Consequently, the lack of well-defined constraints in DNA sequences makes it difficult to develop a robust metric for evaluating their plausibility.

Our observations further highlight this challenge. In our experiments, we found that the novelty values of generated DNA sequences were disproportionately high compared to the initial low-fitness sequences, making the novelty metric less informative. This behavior suggests that DNA sequences tend to diverge significantly from their starting points during optimization, regardless of their biological relevance or plausibility. Due to these limitations, we exclude the *Novelty* metric and instead focus on evaluating the generated sequences using *Fitness* and *Diversity* metrics, which better capture the optimization objectives for CRE design.

H LIMITATIONS

Our ultimate goal is to optimize CREs with higher fitness values than those currently observed. However, the reliability of such optimized CREs is limited by the fact that our oracles are trained on existing real-world datasets. As a result, predictions for CREs with fitness values beyond the training data range may be less accurate. Currently, our primary *in-silico* experiments simulate an optimization setting that starts from low-fitness CREs, following the strategy proposed in (Lee et al., 2024). Previous studies, such as Vaishnav et al. (2022); de Almeida et al. (2024), have successfully designed CREs using simple optimization methods and validated them *in vivo*, demonstrating high fitness and cell-type specificity in real-world scenarios. Our work serves as a complementary effort to these studies by providing advanced algorithmic strategies for CRE optimization. In the future, we hope to conduct *in vivo* experiments to validate the performance of more sophisticated CRE optimization algorithms.

I DETAILS OF RL

I.1 ALGORITHM OVERVIEW

The overview of our algorithm TACO is shown in Alg. 1.

I.2 THE EFFECT OF SUPPORTING RL DESIGNS

As in Fig. 7, we evaluate two main components of our minor designs: the hill-climb replay buffer and entropy regularization. First, we test the effect of the hill-climb replay buffer, which stores past experiences with high fitness values. We find that incorporating a replay buffer significantly enhances the maximum fitness values explored, consistent with observations from prior studies (Lee et al., 2024; Ghugare et al., 2024). Next, we explored the use of entropy regularization, which is designed to encourage exploration by increasing the randomness of the policy and preventing premature convergence to suboptimal actions. Our experiments demonstrate that this approach leads to improved action diversity, highlighting its effectiveness in promoting a broader exploration space.

J OFFLINE MODEL-BASED OPTIMIZATION

In Sec. 4.2, we present results under an active learning setting (Lee et al., 2024), which assumes easy access to a perfect oracle for evaluating generated CRE sequences. However, this setting can lead to optimization processes that overfit to an imperfect oracle (trained with observed data).

Here, we consider an alternative offline model-based optimization (MBO) setting (Reddy et al., 2024), which assumes that accessing the true oracle is costly, but some labeled offline data is available. In this setting, a surrogate model is trained on the offline dataset to guide the optimization process, and the final sequences are evaluated by the oracle. This approach helps mitigate overfitting to a "man-made oracle" trained on limited data.

Algorithm 1 TACO: RL-Based Fine-tuning for Autoregressive DNA Models

Require: Low-fitness dataset $\mathcal{D}^*$, TFBS vocabulary $\mathcal{T}$, Oracle q_θ, Pretrained AR model π_θ, Number of Optimization Rounds E

Preprocessing:
Train LightGBM model on TFBS frequency features $\mathbf{h}(x)$ from dataset $\mathcal{D}^*$
Compute SHAP values $\phi_i(x)$ for each TFBS t_i
Update TFBS rewards $r_{\text{TFBS}}(t)$ based on equation 5
for round $e = 1$ to E **do**
  Sample a batch of sequences $\{x_i\}$ from policy π_θ
  for each sequence x_i **do**
    for time step $t = 1$ to L **do**
      Generate nucleotide a_t using $\pi_\theta(a_t|a_{<t})$
      Observe state $s_t = (a_1, \ldots, a_{t-1})$
      if a_t results in TFBS $t \in \mathcal{T}$ **then**
        Assign reward $r(s_t, a_t) \leftarrow r_{\text{TFBS}}(t)$
      else
        Assign reward $r(s_t, a_t) \leftarrow 0$
      end if
    end for
    Obtain fitness reward r_{fitness} from oracle $q_\theta(x_i)$
    Compute total reward $R \leftarrow \sum_{t=1}^{L} r(s_t, a_t) + r_{\text{fitness}}$
  end for
  Update policy π_θ using REINFORCE:

$$\theta \leftarrow \theta + \alpha \nabla_\theta \mathbb{E}_{\pi_\theta}[R \log \pi_\theta(a_t|s_t)]$$

end for

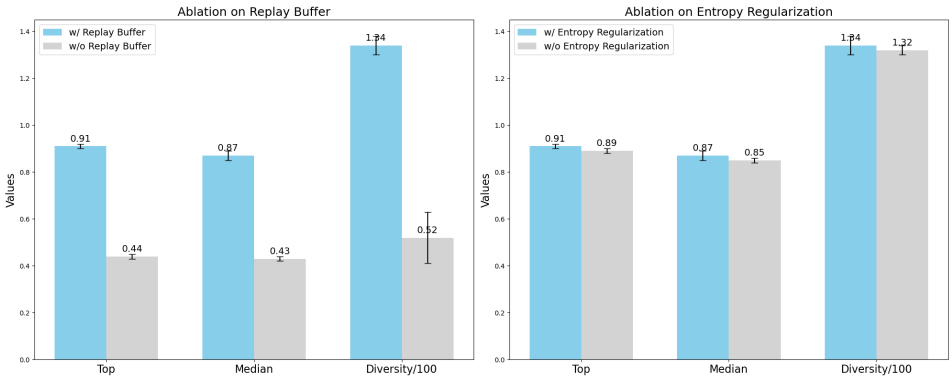

Figure 7: Ablation study on supporting RL designs.

Fig. 8 illustrates an example (a single run on the yeast complex dataset). The left panel shows the curve of the Top fitness predicted by the surrogate as the iterations progress. Since the optimization is guided by the surrogate, the curve continues to increase. Initially, the right panel (representing the Top fitness as predicted by the oracle) also rises steadily. However, around iteration 80, there is a sharp increase in the surrogate's predicted fitness, while the oracle's predicted fitness exhibits a brief spike before declining.

This behavior suggests that at 80 iterations, the optimization process discovers a seemingly high-fitness point. However, the surrogate, believing this direction to be correct, continues optimizing, leading to an overestimation of the fitness. The oracle's actual score, however, does not continue to increase significantly. This example demonstrates that in real optimization processes, the surrogate can be misled by spurious data points, further emphasizing the importance of the offline MBO setting.

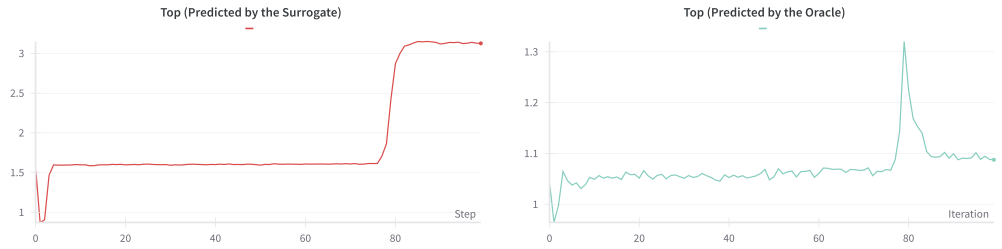

Figure 8: Left: The curve of Top fitness predicted by the surrogate during iterations. Right: The corresponding Top fitness predicted by the oracle. The discrepancy highlights the potential for the surrogate to overestimate fitness due to spurious data points, emphasizing the need for offline MBO settings.

Specifically, we still use the oracle trained in Section 4.1 for the final evaluation of sequences, but we sub-sample a portion of the data to create a predefined offline dataset. The sub-sampling strategy involves randomly splitting the dataset in half and selecting sequences with fitness values below the 95th percentile to simulate a real-world scenario where observed data may have a lower ceiling. This dataset is referred to as D_{offline}. A surrogate model is trained on D_{offline}, and the optimization process proceeds similarly to Section 4.1, except that each iteration is guided by the surrogate, with the oracle used only for final quality evaluation of the generated sequences.

K Motif-based Machine Learning in AI4Science

Motifs are often regarded as small, critical elements in scientific data, such as functional groups in molecules or TFBS in DNA sequences. In machine learning, explicitly modeling these motifs can provide significant benefits. For example, motifs have been successfully used in molecular optimization (Jin et al., 2020; Chen et al., 2021), molecular generation Geng et al., molecular property prediction (Zhang et al., 2021), and DNA language models (An et al., 2022). In the context of DNA CREs, TFBS are widely considered the most important motifs. TFBS typically exhibit cell-type specificity, i.e., the same TFBS may play different roles in different cell types. Our approach is inspired by de Almeida et al. (2024), who observed that during direct evolution guided by an oracle, there is a tendency to first remove repressor TFBS and subsequently add enhancer TFBS to optimize the sequences.

Initially, we intended not to rely on pre-defined motifs from databases. Instead, our goal was to iteratively learn potential motifs in a data-driven manner and use these motifs to enhance the fitness of generated sequences, similar to the idea behind the EM algorithm, which has been explored in molecule optimization (Chen et al., 2021). However, while extracting motifs from molecular graphs is relatively straightforward due to their clear structural boundaries, DNA sequences lack explicit boundaries, making it significantly more challenging to automatically identify meaningful motifs. Nevertheless, recent advancements in understanding promoter mechanisms (Dudnyk et al., 2024) may provide valuable insights for revisiting this idea. That said, even in molecule optimization, where advanced automatic motif mining methods (Geng et al.) are available, the use of pre-defined motifs has been consistently demonstrated to be highly effective (Wu et al., 2023). Therefore, we do not view the reliance on pre-defined motifs as a significant limitation.

L Details of Conditional Generative Models

Although the objectives of generative models and optimization methods differ, both aim to propose samples that deviate from the observed real-world data. To this end, we include a discussion and comparison with SOTA generative models.

Let the data distribution be denoted as $P(x)$, where each data point x is paired with a label y (e.g., the fitness of a CRE). The full dataset observed in the real world is represented as $D = \{(x_i, y_i)\}_{i=1}^{N}$. In biological sequence data, x typically follows a reasonable underlying distribution $P(x)$, which can be approximated using a generative model $P_{\text{pre}}(x)$ without requiring knowledge of y. However,

directly sampling from $P_{\text{pre}}(x)$ often yields sequences with low fitness, as the distribution of y values (e.g., high-fitness regions) is typically narrow and sparsely represented in the data. Thus, an unconditional generative model is generally ineffective for designing biological sequences.

To address this limitation, conditional generative modeling can be employed. By training a model to approximate $P(x \mid y)$ using the offline labeled dataset D, we can condition on high observed fitness values y to theoretically generate high-fitness sequences. Formally, given a dataset where y is partitioned into discrete bins or ranges (e.g., high-fitness values), the conditional generative model is trained to maximize the likelihood.

Subsequently, sequences are generated by sampling x conditioned on y values corresponding to high fitness. However, in practice, this approach often underperforms because the distribution of high y values is extremely narrow, and the model struggles to accurately capture this region.

We compare our method against recent generative models, including the autoregressive generative model reglm (Lal et al., 2024) and the discrete diffusion model DDSM (Avdeyev et al., 2023). For evaluations, we adopted conditional generation strategies for both models. Specifically: **regLM**: The official pretrained weights were used. Sequences were generated by conditioning on the prefix label corresponding to the highest fitness score in each dataset. **DDSM**: This model was trained on our offline dataset, where labels above the 95th percentile were set to $y = 1$, and the remaining labels were set to $y = 0$. The conditional diffusion model was then trained using this binary labeling scheme, and sequences were generated by conditioning on $y = 1$ for evaluation.

As shown in Tab. 15, both regLM and DDSM exhibit high diversity in their generated sequences but fail to match the fitness values achieved by optimization-based methods. This limitation arises because generative models are designed to fit the observed data distribution $P(x \mid y)$, and as such, their generated sequences are inherently constrained by the data's fitness distribution. It is also worth noting that reglm utilized official pretrained weights, which may have been exposed to data with higher fitness scores than our offline dataset. Even with this advantage, it fails to outperform optimization-based methods. In contrast, our method builds upon a pretrained distribution $P_{\text{pre}}(x)$ and further proposes new sequences by iteratively optimizing $P_{\text{pre}}(x)$ through feedback from an oracle or surrogate. The ultimate goal is to reshape the distribution so that high-fitness sequences become more accessible during sampling.

M More Experimental Resutls

Since many conclusions are consistent across different datasets and settings, we have included a significant portion of the experimental results in the appendix.

The complete experimental results for yeast under the oracle-guided optimization setting are presented in Fig. 11. The results for offline MBO are detailed in Tab. 12, Tab. 13, Tab. 14, Tab. 15, and Tab. 16.

Yeast Promoter (Complex)									
Method	**easy**			**middle**			**hard**		
	Top ↑	**Medium ↑**	**Diversity ↑**	**Top ↑**	**Medium ↑**	**Diversity ↑**	**Top ↑**	**Medium ↑**	**Diversity ↑**
PEX	1	1	8.6 (1.14)	1	1	8.4 (1.95)	1	1	9.8 (1.48)
AdaLead	1	1	8.8 (1.3)	1	1	9.0 (1.58)	1	1	7.6 (0.89)
BO	1	1	23.4 (1.52)	1	1	22.6 (1.34)	1	1	25.0 (5.57)
CMAES	1	0.78 (0.13)	30.2 (2.68)	1	0.85 (0.02)	29.4 (1.52)	1	0.79 (0.09)	30.0 (2.5)
DNARL	1	1	8.6 (2.14)	1	1	10.2 (1.14)	1	1	7.7 (0.48)
TACO	1	1	**52.2** (1.92)	1	1	**48.8** (5.36)	1	1	**52.8** (2.77)

Yeast Promoter (Defined)									
Method	**easy**			**middle**			**hard**		
	Top ↑	**Medium ↑**	**Diversity ↑**	**Top ↑**	**Medium ↑**	**Diversity ↑**	**Top ↑**	**Medium ↑**	**Diversity ↑**
PEX	1	1	9.2 (0.84)	1	1	9.2 (1.79)	1	1	9.8 (2.59)
AdaLead	1	1	8.0 (2.35)	1	1	7.0 (1.0)	1	1	6.4 (0.55)
BO	1	1	23.0 (1.58)	1	1	22.8 (2.28)	1	1	23.0 (1.87)
CMAES	1	0.26 (0.36)	30.0 (2.92)	1	0.48 (0.17)	29.8 (1.3)	1	0.44 (0.33)	30.4 (2.3)
DNARL	1	1	11.6 (3.04)	1	1	18.5 (3.0)	1	1	10.2 (1.14)
TACO	1	1	**43.2** (2.77)	1	1	**47.0** (4.64)	1	1	**49.6** (3.65)

Table 11: Performance comparison on yeast promoter datasets (Guided by the Oracle).

Model	**Top ↑**	**Medium ↑**	**Diversity ↑**	**Emb Similarity ↓**
PEX	1.16 (0.09)	1.12 (0.08)	11.4 (57.60)	0.98 (0.01)
AdaLead	1.06 (0.02)	1.00 (0.02)	57.6 (0.55)	0.95 (0.00)
BO	1.09 (0.02)	1.03 (0.03)	24.4 (4.77)	0.97 (0.01)
CMAES	1.06 (0.07)	0.70 (0.12)	29.20 (0.45)	0.75 (0.05)
regLM	1.02 (0.00)	0.94 (0.00)	59.00 (0.00)	0.91 (0.01)
ddsm	0.94 (0.02)	0.79 (0.01)	58.20 (0.40)	0.81 (0.01)
TACO	1.06 (0.01)	0.98 (0.01)	57.4 (1.34)	0.93 (0.01)

Table 12: Offline MBO (95 Percentile) results (yeast promoter, complex).

Model	**Top ↑**	**Medium ↑**	**Diversity ↑**	**Emb Similarity ↓**
PEX	1.19 (0.15)	1.10 (0.16)	10.40 (2.61)	0.98 (0.01)
AdaLead	1.02 (0.04)	0.98 (0.04)	8.20 (1.79)	0.98 (0.01)
BO	1.06 (0.03)	1.02 (0.02)	26.00 (2.24)	0.97 (0.01)
CMAES	0.79 (0.10)	0.39 (0.12)	30.80 (2.05)	0.59 (0.05)
regLM	0.98 (0.01)	0.89 (0.01)	58.80 (0.40)	0.90 (0.00)
DDSM	0.92 (0.02)	0.81 (0.00)	56.20 (0.40)	0.86 (0.01)
TACO	1.10 (0.05)	1.03 (0.04)	46.00 (1.87)	0.97 (0.01)

Table 13: Offline MBO (95 Percentile) results (yeast promoter, defined).

Model	Top ↑	Medium ↑	Diversity ↑	Emb Similarity ↓
PEX	0.75 (0.01)	0.73 (0.01)	13.6 (4.51)	0.98 (0.01)
AdaLead	0.59 (0.01)	0.52 (0.04)	34.2 (59.15)	0.84 (0.16)
BO	0.65 (0.09)	0.61 (0.10)	40.2 (6.14)	0.83 (0.13)
CMAES	0.57 (0.03)	0.41 (0.03)	77.2 (2.28)	0.45 (0.04)
regLM	0.65 (0.01)	0.48 (0.02)	150.00 (0.00)	0.28 (0.02)
DDSM	0.41 (0.00)	0.41 (0.00)	15.40 (0.49)	0.99 (0.00)
TACO	0.69 (0.03)	0.60 (0.05)	141.2 (1.92)	0.82 (0.05)

Table 14: Offline MBO (95 Percentile) results (human enhancer, HepG2).

Model	Top ↑	Medium ↑	Diversity ↑	Emb Similarity ↓
PEX	0.76 (0.02)	0.73 (0.02)	15.8 (4.97)	0.97 (0.01)
AdaLead	0.66 (0.08)	0.58 (0.06)	63.2 (70.01)	0.88 (0.12)
BO	0.71 (0.07)	0.64 (0.08)	43.6 (6.91)	0.87 (0.04)
CMAES	0.66 (0.02)	0.44 (0.03)	79.2 (3.83)	0.35 (0.03)
regLM	0.69 (0.02)	0.47 (0.01)	149.60 (0.49)	0.38 (0.02)
DDSM	0.43 (0.00)	0.40 (0.00)	93.40 (0.49)	0.80 (0.00)
TACO	0.75 (0.09)	0.72 (0.10)	102.6 (20.14)	0.97 (0.04)

Table 15: Offline MBO (95 Percentile) results (human enhancer, K562).

Model	Top ↑	Medium ↑	Diversity ↑	Emb Similarity ↓
PEX	0.69 (0.01)	0.68 (0.00)	17.8 (3.90)	0.98 (0.01)
AdaLead	0.59 (0.08)	0.56 (0.08)	8.6 (2.30)	0.96 (0.03)
BO	0.61 (0.09)	0.52 (0.08)	42.4 (4.77)	0.80 (0.08)
CMAES	0.58 (0.05)	0.42 (0.03)	78.6 (1.14)	0.40 (0.06)
regLM	0.61 (0.00)	0.47 (0.01)	149.60 (0.49)	0.38 (0.03)
DDSM	0.54 (0.00)	0.49 (0.00)	102.20 (1.17)	0.91 (0.01)
TACO	0.68 (0.08)	0.62 (0.08)	121.4 (7.86)	0.90 (0.03)

Table 16: Offline MBO (95 Percentile) results (human enhancer, S-KN-SH).

N Analysis of Gradient Ascent's performance in offline MBO settings.

As stated in Reddy et al. (2024), in offline MBO settings, directly applying Gradient Ascent (GAs) to a surrogate is theoretically expected to generate adversarial examples with poor performance. However, in our current CRE dataset, we did not observe this phenomenon. Instead, directly performing GAs yields surprisingly good results. This is indeed a surprising observation. To the best of our knowledge, prior CRE design work has not extensively explored GAs methods, except for Reddy et al. (2024). However, Reddy et al. (2024) does not seem to include an ablation study on regularization terms. Therefore, in the context of DNA CRE design—where Enformer-based models (Avsec et al., 2021) are widely used to train scoring functions—it remains an open question whether directly applying GAs to a differentiable surrogate would result in adversarial examples with poor performance. We acknowledge that in the case of a perfect oracle, adversarial examples would likely emerge. However, due to the simple data partitioning strategies commonly used in this field, it appears that a surrogate trained on a subset can sufficiently approximate the oracle.

To further address this concern, we validated GAs performance across different fitness quantiles (95 shown in Fig 9, 80 shown in Fig. 10, 60 shown in Fig. 11) using K562 cells (our default setting was

the 95th percentile). Our GAs implementation directly operates on the one-hot encoded probability simplex following Reddy et al. (2024), which allows for smooth updates during optimization. Therefore, we report both the results on the one-hot-encoded simplex (**Prob**) and the hard-decoded sequences optimized (**Sequence**) in each iteration. We reported the scores predicted by both the surrogate and oracle for these two representations. Our findings indicate: 1. For the 95th percentile, as shown in Fig. 9, the fitness in the sequence space initially rises sharply but then drops. For the 60th percentile, as shown in Fig. 11, a similar pattern is observed in the oracle's predictions within the Prob space. This reveals **a gap between the surrogate and the oracle**, as the surrogate's predictions consistently increase. This aligns with our expectations of the offline MBO setting, i.e., the surrogate cannot fully reflect the oracle. 2. However, the oracle's predictions do show significant improvement at the start, indicating that directly applying GAs to the surrogate can still benefit the oracle's results. This suggests that, under the current CRE data partitioning strategy, even a surrogate trained on low-fitness subsets can reasonably capture the trends of the oracle's predictions (although the surrogate itself, having never encountered high-fitness data, predicts much lower upper bounds).

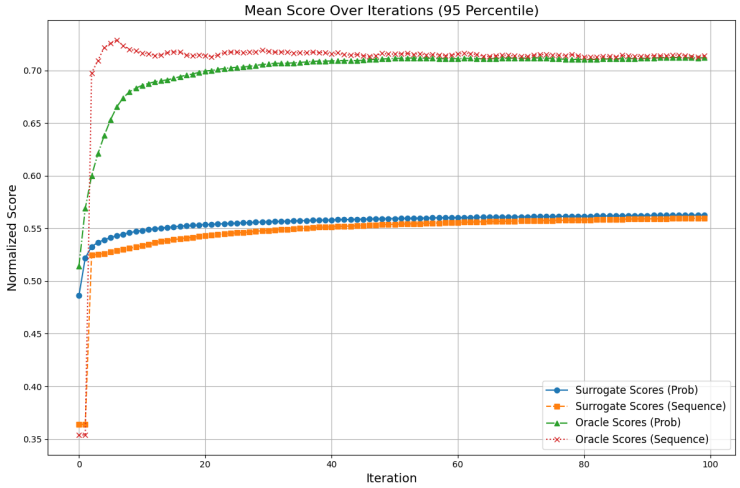

Figure 9: Results of GAs using the 95th percentile subset.

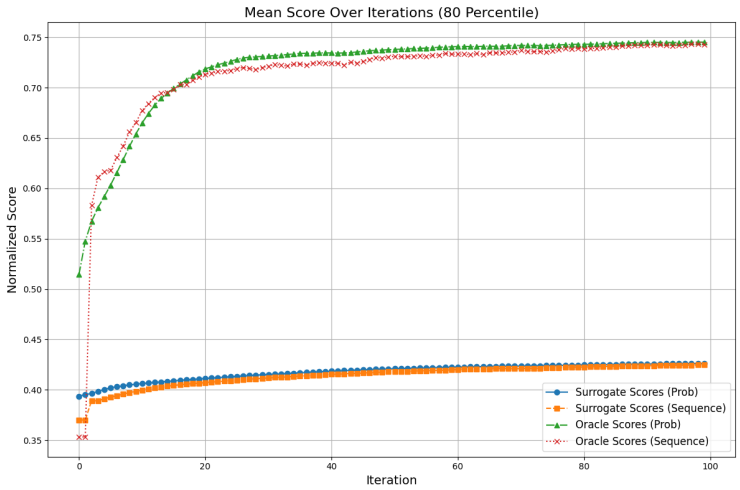

Figure 10: Results of GAs using the 80th percentile subset.

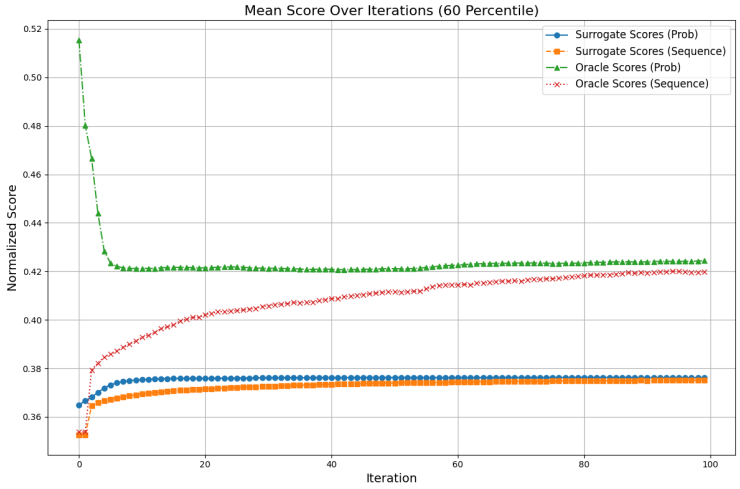

Figure 11: Results of GAs using the 60th percentile subset.

Based on the current evidence, we believe that the observed good performance of GAs may be an inherent property (possibly related to the inherent data distribution of CREs and our current data partitioning strategy). Even a surrogate trained on the 60th percentile subset can achieve decent performance. This is an interesting question for future research in CRE design.

However, we emphasize that our primary focus is on designing optimization algorithms rather than relying on **a differentiable surrogate**. Our current offline MBO setting has already made the task more challenging, achieving the intended goal of designing an offline MBO setting. Nevertheless, we do not yet fully understand why GAs does not lead to significantly poor results. Figuring this out is left for future work, but I believe it is crucial for machine-learning-driven CRE design.

Besidies, we have also added the results of different methods (including GAs) guided by a surrogate trained on the 60th percentile shown in Tab. 17, Tab. 18 and Tab. 19. It can be observed that, despite the significant gap between the surrogate and the oracle under the 60th percentile training, GAs still achieves relatively good performance. Notably, under the 60th percentile setting, PEX, which performed well at the 95th percentile, shows moderate results, while CMAES, which previously performed the worst, achieves excellent performance. Our TACO, in this setting, continues to maintain SOTA results.

Model	Top ↑	Medium ↑	Diversity ↑	Emb Similarity ↓
PEX	0.54 (0.02)	0.48 (0.02)	16.4 (5.13)	0.80 (0.03)
AdaLead	0.50 (0.05)	0.42 (0.02)	**146.6** (2.61)	**0.36** (0.03)
BO	0.46 (0.04)	0.41 (0.02)	41.2 (6.91)	0.71 (0.07)
CMAES	0.55 (0.04)	0.41 (0.02)	78.4 (3.97)	0.41 (0.05)
GAs	0.59 (0.01)	0.51 (0.01)	136.20 (0.40)	0.80 (0.01)
TACO	**0.56** (0.08)	**0.50** (0.08)	134.6 (14.03)	0.77 (0.08)

Table 17: Results of HepG2 (60 Percentile).

Model	Top ↑	Medium ↑	Diversity ↑	Emb Similarity ↓
PEX	0.50 (0.06)	0.45 (0.04)	13.6 (2.19)	0.87 (0.02)
AdaLead	0.62 (0.09)	**0.49** (0.10)	**138.6** (20.7)	**0.55** (0.11)
BO	0.55 (0.03)	0.44 (0.03)	43.6 (7.37)	0.66 (0.11)
CMAES	**0.66** (0.07)	0.47 (0.05)	79.0 (4.36)	0.49 (0.06)
GAs	0.52 (0.02)	0.43 (0.00)	126.60 (1.20)	0.84 (0.01)
TACO	0.63 (0.04)	0.48 (0.02)	132.4 (25.7)	0.62 (0.21)

Table 18: Results of K562 (60 Percentile).

Model	Top ↑	Medium ↑	Diversity ↑	Emb Similarity ↓
PEX	0.50 (0.11)	0.47 (0.11)	19.6 (3.21)	0.74 (0.04)
AdaLead	0.55 (0.06)	0.44 (0.03)	**141.6** (13.24)	0.54 (0.09)
BO	0.55 (0.09)	0.46 (0.05)	48.8 (11.65)	0.72 (0.09)
CMAES	0.61 (0.09)	0.44 (0.03)	75.2 (1.92)	**0.50** (0.05)
GAs	0.48 (0.01)	0.42 (0.00)	140.00 (0.63)	0.59 (0.01)
TACO	**0.69** (0.04)	**0.57** (0.06)	135.6 (5.5)	0.78 (0.06)

Table 19: Results of S-KN-SH (60 Percentile).